HHS Public Access

Author manuscript

Cell Rep. Author manuscript; available in PMC 2019 December 16.

Published in final edited form as:

Cell Rep. 2019 March 19; 26(12): 3298–3312.e4. doi:10.1016/j.celrep.2019.02.080.

Ndfip Proteins Target Robo Receptors for Degradation and Allow Commissural Axons to Cross the Midline in the Developing Spinal Cord

Madhavi Gorla[1], **Celine Santiago**[1], **Karina Chaudhari**[1], **Awo Akosua Kesewa Layman**[2,3], **Paula M. Oliver**[2,3], **Greg J. Bashaw**[1,4,*]

[1]Department of Neuroscience, Perelman School of Medicine, University of Pennsylvania, Philadelphia, PA 19104, USA

[2]The Children's Hospital of Philadelphia, Division of Protective Immunity, 3615 Civic Center Boulevard, Philadelphia, PA 19104, USA

[3]Department of Pathology and Laboratory Medicine, Perelman School of Medicine, University of Pennsylvania, 3400 Civic Center Boulevard, Building 421, Philadelphia, PA 19104, USA

[4]Lead Contact

SUMMARY

Commissural axons initially respond to attractive signals at the midline, but once they cross, they become sensitive to repulsive cues. This switch prevents axons from re-entering the midline. In insects and mammals, negative regulation of Roundabout (Robo) receptors prevents premature response to the midline repellant Slit. In *Drosophila,* the endosomal protein Commissureless (Comm) prevents Robo1 surface expression before midline crossing by diverting Robo1 into late endosomes. Notably, Comm is not conserved in vertebrates. We identified two Nedd-4-interacting proteins, Ndfip1 and Ndfip2, that act analogously to Comm to localize Robo1 to endosomes. Ndfip proteins recruit Nedd4 E3 ubiquitin ligases to promote Robo1 ubiquitylation and degradation. Ndfip proteins are expressed in commissural axons in the developing spinal cord and removal of Ndfip proteins results in increased Robo1 expression and reduced midline crossing. Our results define a conserved Robo1 intracellular sorting mechanism between flies and mammals to avoid premature responsiveness to Slit.

Graphical Abstract

*Correspondence: gbashaw@pennmedicine.upenn.edu.

AUTHOR CONTRIBUTIONS

M.G. designed and performed all of the *in vitro* experiments and wrote the paper. M.G. designed and performed the experiments and analysis of *in vivo* expression patterns and phenotypes of Ndfip proteins. C.S. contributed to the experiments to analyze Ndfip1 mutants and expression patterns. K.C. contributed to the DiI injection experiments in Ndfip mutant spinal cords. A.A.K.L. and P.M.O. performed timed breeding experiments and provided embryonic and adult mouse tissue from Ndfip1 mutants and controls. G.J.B. designed the experiments, wrote the paper, and supervised the project.

DECLARATION OF INTERESTS

The authors declare no competing interests.

SUPPLEMENTAL INFORMATION

Supplemental Information can be found with this article online at https://doi.org/10.1016/j.celrep.2019.02.080.

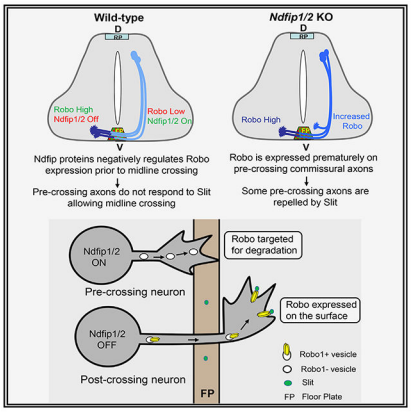

In Brief

In order to cross the midline in the developing spinal cord, commissural axons must prevent premature responses to the midline repellant Slit. Here Gorla et al. define a key role for the Ndfip adaptor proteins in preventing the surface expression of the Robo1 receptor prior to midline crossing.

INTRODUCTION

During the development of the nervous system in bilaterally symmetric animals, many neurons extend their axons across the midline in order to establish neural circuits that are essential for cognitive functions and motor behavior (Dickson and Zou, 2010; Neuhaus-Follini and Bashaw, 2015a; Vallstedt and Kullander, 2013). In both the ventral nerve cord of invertebrates and the mammalian spinal cord, midline crossing is controlled by a balance of attractive and repulsive signals through the interaction between growth cone receptors and ligands secreted by the midline and other cells (Evans and Bashaw, 2010). Growing commissural axons initially respond to attractive signals, which include members of the Netrin and Sonic Hedgehog families (Charron et al., 2003; Ishii et al., 1992; Mitchell et al., 1996; Serafini et al., 1996). Once across the midline, commissural axons become sensitive to repellents, which include Slit and Semaphorin proteins (Brose et al., 1999; Kidd et al., 1999; Zou et al., 2000). This switch prevents commissural axons from re-entering the midline and allows them to turn longitudinally and ultimately reach their synaptic targets. In humans, defects in midline axon guidance have been implicated in multiple neurodevelopmental disorders such as horizontal gaze palsy with progressive scoliosis, congenital mirror movements, and autism spectrum disorders (Blockus and Chédotal, 2014; Engle, 2010; Jamuar et al., 2017; Jen et al., 2004).

The secreted Slit ligands and their Roundabout (Robo) receptors mediate repulsive axon guidance at the midline, and this function is highly conserved in both invertebrates and vertebrates (Dickson and Zou, 2010). Axons expressing Robo receptors are repelled from the midline in response to the repulsive ligand Slit, which is secreted from the midline. In both insects and mammals, prior to crossing the midline, commissural axons prevent premature responsiveness to Slit by regulating the expression and activity of Robo receptors

(Evans et al., 2015; Keleman et al., 2002; Sabatier et al., 2004). In *Drosophila,* a major mechanism that regulates repulsive signaling in pre-crossing axons is the negative regulation of Robo1 surface expression by Commissureless (Comm) (Keleman et al., 2002; Kidd et al., 1998; Tear et al., 1996). Comm inhibition of Robo repulsion is absolutely required for midline crossing. Prior to midline crossing, Comm expression is upregulated in commissural neurons, in part by a mechanism involving the transcriptional activation function of the Frazzled (Fra) receptor intracellular domain (Neuhaus-Follini and Bashaw, 2015b; Yang et al., 2009). Once commissural axons reach the midline, Comm is downregulated, so that Robo1-dependent Slit sensitivity is re-established, thereby preventing axons from re-crossing. Comm acts by diverting newly synthesized Robo1 into the late endosomal compartment, thus preventing Robo1 expression on the cell surface (Keleman et al., 2002, 2005).

In contrast to Slit ligands and Robo receptors, the *comm* gene is apparently not conserved outside of insects (Evans and Bashaw, 2012; Keleman et al., 2002). This raises the critical question of how Robo1 surface levels are negatively regulated in commissural axons prior to crossing the floor plate in the mammalian spinal cord. Interestingly, in *robo3*−/− mutant mouse embryos, all spinal commissural axons fail to cross the midline, a phenotype resembling *comm* mutants in *Drosophila* (Sabatier et al., 2004). Moreover, the absence of midline crossing in *robo3* mutants can be partially suppressed by the removal of *robo1* (Sabatier et al., 2004). However, and in marked contrast to the role of Comm in *Drosophila,* Robo3 does not localize to endosomes and does not bind to Robo1. Most important, Robo3 does not inhibit Robo1 surface expression on pre-crossing commissural axons (Sabatier et al., 2004). More recent evidence indicates that Robo3 can contribute to midline axon attraction by potentiating the activity of the Netrin-1 receptor DCC, suggesting that the Robo3 phenotype is likely only partially dependent on its ability to inhibit Slit responsiveness (Zelina et al., 2014). Thus, it remains unclear how Robo1 protein levels are kept low on pre-crossing axons in mammals and whether there is a Comm-like mechanism that operates in the developing spinal cord.

Here we report the discovery of a class of mammalian proteins with limited sequence similarity to the functional domain of *Drosophila* Comm that regulate mammalian Robo1 trafficking through an analogous mechanism. The Nedd4-family interacting proteins Ndfip1 (N4WBP5) and Ndfip2 (N4WBP5A) can serve as adaptor proteins to recruit Nedd4 E3 ligases to specific substrate proteins, leading to their ubiquitylation and subsequent degradation (Harvey et al., 2002; Mund and Pelham, 2009, 2010; Shearwin-Whyatt et al., 2004). Besides their role as adaptors, Ndfip proteins also act as activators of E3 ligase enzymatic activity by releasing the Nedd4 ligase from its auto-inhibitory conformation (Mund and Pelham, 2009). In association with their downstream interacting E3 ligases, Ndfip proteins play important roles in regulating T cell differentiation and maturation (Layman et al., 2017; O'Leary et al., 2016; Oliver et al., 2006; Ramon et al., 2012). Several reports also suggest that Ndfip1 has neuronal functions, including regulating cortical development, neurite outgrowth, and dendrite development (Goh et al., 2013; Hammond et al., 2014); however, it is unclear how Ndfip1 regulates these processes.

In this paper we show that, like Comm, Ndfip1 and Ndfip2 can prevent the surface expression of the mammalian Robo1 receptor by recruiting it to late endosomes *in vitro.* In addition to altering Robo1 localization, Ndfip proteins also trigger the ubiquitylation and degradation of the Robo1 receptor. The ability of Ndfip proteins to regulate Robo1 depends on HECT E3 ligases, because point mutations that disrupt the interaction of Ndfip proteins with E3 ligases or pharmacological inhibition of HECT E3 ligase activity result in the failure to reduce surface Robo1 levels. *In vivo,* Ndfip1 and Ndfip2 proteins are detected in commissural axons in the developing spinal cord. Finally, in *Ndfip1* and *Ndfip2* single- and double-knockout mice, Robo1 expression is increased in pre-crossing commissural axons in the spinal cord, and there is a significant reduction in midline crossing. On the basis of these observations, we propose that Ndfip proteins act analogously to *Drosophila* Comm to regulate mammalian Robo1 localization and then lead to receptor degradation through the recruitment of Nedd4-family E3 ubiquitin ligases. This intracellular trafficking mechanism is important to prevent commissural axons from prematurely responding to Slit.

RESULTS

The NEDD4-Family Interacting Proteins Ndfip1 and Ndfip2 Share Similarities with Comm

We sought to identify proteins with any similarity to Comm in mammals by searching for proteins that share features of the short cytoplasmic domain that is conserved between *Drosophila* and mosquito Comm (Keleman et al., 2002). We find that this domain aligns with a region of Nedd4-family interacting proteins Ndfip1 and Ndfip2. These proteins share 60% similarity with the core 25 amino acid functional domain of Comm proteins, but outside of this region there is no obvious sequence similarity (Figure 1A). Ndfip proteins share many additional properties with Comm. Like Comm, Ndfip1 and Ndfip2 are localized to endosomes and have transmembrane domains (Shearwin-Whyatt et al., 2004). In addition, the Ndfip proteins both have cytoplasmic PPXY and LPXY motifs (Mund and Pelham, 2009, 2010). Last, Comm and the Ndfip proteins can both bind to HECT family E3 ubiquitin ligases, although the significance of this interaction for Comm function is unclear (see Discussion). In the case of the Ndfip proteins, it has been shown that they can also recruit these E3 ligases to proteins destined for degradation (Howitt et al., 2012; Mund and Pelham, 2009; Myat et al., 2002).

Ndfip Proteins Regulate the Levels and Localization of Robo1 *In Vitro*

Because Ndfip proteins recruit E3 ubiquitin ligases and target their substrates for degradation, we first tested whether overexpression of these proteins regulates Robo protein levels *in vitro.* Strikingly, we found that expression of Ndfip1 or Ndfip2 reduces Robo1 levels in COS-7 cells (Figures 1B and 1C) compared with control cells (Figure 1F). Interestingly, overexpression of Ndfip proteins has no effect on the steady-state levels of another closely related repulsive receptor, Robo2, indicating the specificity of Ndfip proteins toward Robo1 (Figures S1A–S1C). To test if Ndfip proteins can regulate endogenous Robo1 levels, we transfected HeLa cells with Ndfip1 and Ndfip2 and monitored Robo1 protein levels. Consistent with our observation in COS-7 cells, overexpression of Ndfip1 (Figures 1D and 1G) or Ndfip2 (Figures 1E and 1G) significantly reduces endogenous Robo1 levels but has no effect on the levels of the transmembrane integrin beta-1 receptor, further

supporting the idea that the Ndfip proteins specifically regulate Robo1. To test whether Robo1 levels could be regulated by other PY motif-containing proteins, or if instead this effect is specific to the Ndfip proteins, we also performed similar experiments with Itch (a PY motif-containing E3 ubiquitin ligase) and found that overexpression of Itch has no significant effect on Robo1 levels (Figures S1E and S1G).

Ndfip proteins localize to endosomes and target their substrates for degradation; therefore, we examined whether ectopic expression of Ndfip proteins influence the subcellular localization of Robo1. As expected, when expressed in COS-7 cells, the majority of Robo1 is localized to the plasma membrane (Figure 1H). Remarkably, upon overexpression of either Ndfip1 or Ndfip2, the intensity of plasma membrane localized Robo1 is significantly reduced, and a majority of the perinuclear and cytoplasmic Robo1 is co-localized with Ndfip proteins (Figures 1I and 1J). The distribution of hRobo1 in the presence of Ndfip proteins is quite similar to the distribution of *Drosophila* Robo1 in COS-7 cells overexpressing Comm (Keleman et al., 2002). On the basis of previous studies (Harvey et al., 2002; Shearwin-Whyatt et al., 2004), and our observation that Ndfip proteins predominantly localize to the Rab7 positive late endosomal compartment (Figure S2), these sites of Robo1 and Ndfip co-localization are likely to be late endosomes. Our data indicate that Ndfip1 and Ndfip2 can regulate the levels and localization of Robo1 *in vitro* and suggest that they do so through a mechanism that may be analogous to the way that Comm regulates Robo1 in *Drosophila*.

Because Ndfip proteins serve as adapters between E3 ubiquitin ligases and specific substrate proteins (Foot et al., 2008; Mund and Pelham, 2009), we tested whether Ndfip proteins bind to Robo1. We find that Ndfip1 and Ndfip2 are both coimmunoprecipitated with Robo1, indicating that Robo1 and Ndfip proteins can physically interact (Figures 1K and S3A). To test whether these interactions could be detected under more physiological conditions, we also performed immunoprecipitation from mouse brain homogenates using Ndfip1 and Ndfip2 antibodies and found that Robo1 immunoprecipitated with both Ndfip1 and Ndfip2, indicating that they form a complex *in vivo* (Figures S3B and S3C). Together these results suggest that Ndfip proteins interact with Robo1, potentially leading to its subsequent redistribution and degradation.

Ndfip1 and Ndfip2 Decrease Surface Robo1 Expression

The results described above indicate that Ndfip proteins share Comm's ability to bind to and regulate the subcellular localization and expression levels of Robo1. A key feature of the Comm sorting model is that Comm acts to negatively regulate the surface expression of Robo; therefore, we next examined whether Ndfip proteins also reduce surface expression of Robo1. We monitored the levels of Robo1 present on the plasma membrane by immunostaining prior to fixation and permeabilization. Cells transfected with Robo1 display high levels of Robo1 on the cell surface (Figures 2A and 2A′). In contrast, surface Robo1 intensity is significantly reduced in cells co-expressing Ndfip1 (Figures 2B, 2B′, and 2D) or Ndfip2 (Figures 2C, 2C′, and 2D), indicating that Ndfip proteins can reduce Robo1 surface levels. To more carefully quantify the effect of Ndfip proteins on Robo1 surface expression, we used a surface biotinylation assay. Cells co-expressing Robo1 and Ndfip proteins were subjected to chemical coupling with biotin, and the surface fractions were isolated. In cells

transfected with Robo1 alone, a significant amount of biotinylated Robo1 is present. However, we detect significantly less surface Robo1 in cells transfected with either Ndfip1 or Ndfip2 (Figures 2E and 2F). Together these results provide strong evidence that Ndfip proteins can negatively regulate total and surface Robo1 levels when expressed in heterologous COS-7 cells.

Ndfip1 and Ndfip2 Promote Robo1 Ubiquitylation and Degradation

Given the potent effect of Ndfip proteins on Robo1 localization and surface expression, we sought to determine the biochemical mechanism underlying Ndfip-mediated Robo1 degradation. Previous studies have shown that Ndfip proteins interact with E3 ubiquitin ligases and promote their activity (Mund and Pelham, 2009; Riling et al., 2015). In addition, these proteins also interact with substrate proteins to facilitate the recruitment of E3 ligases, thus promoting ubiquitin dependent degradation (Foot et al., 2008). Because Robo1 levels are reduced upon overexpression of Ndfip proteins, we hypothesized that Ndfip proteins promote Robo1 ubiquitylation, thus marking it for subsequent degradation. To test the ubiquitylation status of Robo1, we co-expressed it with Ndfip proteins and FLAG-tagged ubiquitin and performed immunoprecipitation studies followed by western blot analysis with anti-FLAG antibodies. We observe minimal Robo1 ubiquitylation under basal conditions. Although the amount of ubiquitylated Robo1 varied between cells expressing Ndfip1 and Ndfip2, overexpression of either protein significantly increases Robo1 ubiquitylation compared with basal conditions (Figures S4A and S4B). To investigate the effect of the two major degradative pathways on the fate of ubiquitylated Robo1, we treated the cells with proteasomal (MG132) (Figure S4A) and lysosomal (chloroquine [CQ]) (Figure S4B) inhibitors. To our surprise, ubiquitylated Robo1 is stabilized and detected at higher levels upon treatment with both of these inhibitors (Figures S4A and S4B), indicating the possible involvement of both pathways in clearance of ubiquitylated Robo1.

On the basis of these observations, we reasoned that these inhibitors should also prevent the degradation of Robo1 and stabilize Robo1 protein levels in cells overexpressing Ndfip proteins. Indeed, overexpression of either Ndfip1 or Ndfip2 results in reduced levels of Robo1, while neither Ndfip1 nor Ndfip2 proteins promote Robo1 degradation in cells treated with CQ (Figures S4C–S4E). MG132 treatment significantly restores Robo protein levels in Ndfip1-expressing cells, but it does not restore Robo protein levels in Ndfip2 expressing cells. These results suggest that both proteosomal and lysosomal pathways are involved in Robo1 clearance and that Ndfip2 may selectively target Robo for lysosomal degradation. It is interesting to note that both Ndfip1 and Ndfip2 protein levels are also stabilized upon the treatment with MG132 and CQ. Together, our data provide evidence that Ndfip proteins mark Robo1 for ubiquitin dependent degradation through proteasomal and lysosomal pathways.

Ndfip PY Motifs and E3 Ligase Activity Are Required for Degradation of Robo1

It has been shown that the PY motifs of both Ndfip1 and Ndfip2 are important for their interaction with the WW domains of E3 ubiquitin ligases, and this interaction is also known to enhance E3 ligase activity (Foot et al., 2008; Mund and Pelham, 2009). Therefore, we hypothesized that mutation of the PY motifs in Ndfip1 and Ndfip2 would prevent Robo1

protein re-localization and degradation. To test this idea, we co-expressed Ndfip proteins bearing mutations in their PY motifs with Robo1 in COS-7 cells. Robo1 is strongly expressed on the cell surface and in a perinuclear location in control-transfected cells (Figure 3A), while cells expressing either Ndfip1 or Ndfip2 result in reduced plasma membrane expression of Robo1 and co-localization of Robo and Ndfip proteins in the endosomal compartment (Figures 3B, 3C, and 1). Conversely, co-expression of PY mutant form of Ndfip proteins fails to reduce the plasma membrane localization of Robo1 (Figures 3D and 3E), suggesting that these motifs are critical for Ndfip proteins to regulate Robo1. Mutation of the PY motifs does not appear to significantly alter the localization of the Ndfip proteins themselves, as both proteins are still predominantly co-localized with late endosomal markers (Figure S5); however, the PY mutant form of Ndfip1 is expressed at much higher levels than wild-type Ndfip1, suggesting that preventing its association with HECT ligases leads to stabilization of the protein (Figure 3F).

Next, we used surface biotinylation to measure the amount of Robo1 on the cell surface in COS-7 cells expressing PY mutant forms of Ndfip proteins. Consistent with our previous observations, the amount of surface Robo1 is reduced in cells expressing Ndfip1 and Ndfip2 (Figures 3F and 3G), as indicated by reduced levels of biotinylated Robo1 in these cells. In marked contrast, biotinylated Robo1 levels are significantly restored in cells transfected with PY mutant forms of either Ndfip1 (Figure 3F) or Ndfip2 (Figure 3G). It is interesting to note that PY mutated Ndfip1 completely restores cell surface Robo1, while PY mutated Ndfip2 results only in a partial restoration of surface Robo1, suggesting that the mutant version of Ndfip2 still retains some ability to regulate Robo1. Importantly, total Robo1 protein levels are also significantly restored in cells transfected with PY mutant forms of either Ndfip1 (Figures 3F and 3J) or Ndfip2 (Figures 3G and 3K). This suggests that the ability of Ndfip proteins to recruit HECT E3 ligases through their PY motifs is required for Ndfip proteins to reduce Robo1 receptor levels at the cell surface (Figure 3L).

Ndfip1 and Ndfip2 enhance the catalytic activity of HECT domain containing E3 ubiquitin ligases by inducing conformational changes (Mund and Pelham, 2009). Because overexpression of Ndfip proteins promotes ubiquitylation of Robo1 (as shown in Figures S4A and S4B), we reasoned that HECT E3 ligase activity should also be required for the regulation of Robo1 levels. In order to test this prediction, we used a specific HECT ligase small molecule inhibitor, Heclin, which inhibits several HECT ligases in cultured cells (Mund et al., 2014). We measured the level of Robo1 ubiquitylation and degradation in Ndfip1 and Ndfip2 transfected COS-7 cells in the presence or absence of Heclin. As shown in Figure 3H, the amount of Robo1 ubiquitylation is strongly increased in both Ndfip1 and Ndfip2-transfected cells. However, Robo1 ubiquitylation is significantly attenuated in cells that are treated with Heclin (Figure 3H). Likewise, Heclin also inhibits degradation of Robo1 in cells expressing Ndfip1 and Ndfip2 (Figures 3I–3K), indicating the importance of HECT E3 ligase activity in Ndfip-mediated Robo1 degradation. Collectively, our data provide compelling evidence that the PY motifs of Ndfip proteins and an active HECT E3 ubiquitin ligase complex are important for the regulation of Ndfip-dependent Robo1 turnover *in vitro* (Figure 3M).

Ndfip1 and Ndfip2 Are Expressed in Spinal Commissural Neurons

To examine potential *in vivo* roles for the Ndfip proteins during axon guidance, we first performed mRNA *in situ* analysis to examine Ndfip transcript expression during embryonic stages when spinal commissural axons are growing toward and crossing the floor plate (Figure 4). Both Ndfip1 and Ndfip2 transcripts are specifically and robustly expressed in E10.5 and E11.5 spinal cords (Figures 4A and 4B). Ndfip1 is enriched in the floor plate region, motor column and in the dorsal root ganglia (DRG), while Ndfip2 mRNA appears to be more uniformly expressed. Expression of both Ndfip1 and Ndfip2 mRNA is higher in E11.5, and signal is detected in the dorsal spinal cord in areas occupied by commissural neurons (Figures 4A and 4B, arrows). These patterns of mRNA expression are specific, as no signal is detected using sense control probes and specific signals are absent in sections from *Ndfip* mutants (Figure S6).

Antibody staining reveals that Ndfip1 is strongly expressed in the region of the floor plate during embryonic stages E10.5–E12.5 (Figure 4C). In addition, we also observe Ndfip1 signal in motor neurons and in the DRG. Co-localization of Ndfip1 with TAG1, a cell surface protein that is expressed on pre-crossing commissural axons, indicates that Ndfip1 is expressed within a subset of commissural axons, which can be detected at both E10.5 and E11.5 (Figures 4E and 4F). Intriguingly, like TAG1, Ndfip1 protein is not detected at high levels in post-crossing commissural axons, as shown by complementary domains of expression for Ndfip1 and Robo1 (Figure 4G). Additional co-labeling experiments with Ndfip1 and DCC, Robo3, and L1CAM also support the conclusion that Ndfip1 is enriched in the pre-crossing portions of commissural axons (Figure S7). This pattern of expression is consistent with a potential role in the transient regulation of Robo1 surface expression. Importantly, Ndfip1 protein expression is decreased in spinal cord sections from Ndfip1 mutants at all stages examined (E10.5, E11.5, and E12.5) (Figure S6). Because existing Ndfip2 antibodies do not work well for immunohistochemistry on tissue sections, we took advantage of the fact that the Ndfip2 mutants were generated by replacing the Ndfip2 coding sequence with a GFP reporter (O'Leary et al., 2016). Examination of GFP expression in Ndfip2-GFP heterozygous mice reveals strong expression of Ndfip2 during stages when spinal commissural axons are growing toward and crossing the floor plate (Figure 4D). Co-labeling with GFP and TAG1 or DCC reveals clear expression in commissural neurons at E10.5 and E11.5 (Figures 4H–4J). Because we are detecting Ndfip2 expression with the GFP reporter, it is unclear whether, like Ndfip1, Ndfip2 protein is also enriched in pre-crossing commissural axons: we can only conclude that Ndfip2 is indeed expressed in commissural neurons at these stages. To further explore the expression of Ndfip proteins in commissural axons, we generated primary cultures of dorsal spinal cord neurons from E12.5 wild-type mice and co-labeled for Ndfip1 and either DCC or TAG1. In both cases we observe clear Ndfip1 expression in DCC and TAG1-positive dorsal commissural axons (Figures 4K and 4L).

Ndfip1 and *Ndfip2* Mutants Show a Reduction in Midline Crossing

To examine the role of Ndfip proteins in commissural axon guidance, we analyzed embryonic spinal commissural axons in *Ndfip1*- and *Ndfip2*-knockout mice. Ndfip1 mutants were generated by the insertion of a gene trap vector in the Ndfip1 locus, which results in

disruption of the *Ndfip1* gene (Oliver et al., 2006). On the basis of analysis of Ndfip1 transcripts in these mice, the gene trap insertion was demonstrated to completely abolish Ndfip1 expression (Oliver et al., 2006). *Ndfip2* mutant mice were generated by replacing the Ndfip2 coding sequence with a GFP reporter as described above. RNA *in situ* analysis on Ndfip1 and Ndfip2 mutants and controls indicates that these mutants completely remove Ndfip transcripts, and using an anti-Ndfip1 antibody, we further confirmed that the overall signal for Ndfip1 is reduced in *Ndfip1* mutant embryonic spinal cords compared with wild-type embryos (Figure S6). We analyzed commissural axon guidance defects in *Ndfip* mutant embryos by immunostaining transverse sections of the spinal cord with antibodies to the commissural axon markers, TAG1 and Robo3. There is a significant reduction in TAG1-positive commissural axons crossing the floor plate at the ventral midline in *Ndfip1* and *Ndfip2* mutant embryos at E10.5 (Figures 5A, 5C, and 5E). There is also a significant decrease in the thickness of Robo3-positive commissural axon bundle crossing the floor plate in both mutants at E10.5 (Figures 5B, 5D, and 5F). At E11.5, the reduction of both TAG1-positive and Robo3-positive commissure thickness in *Ndfip1* and *Ndfip2* mutant embryos is more modest, but it is still significantly different from littermate controls (Figure S8). Interestingly, Robo3-positive pre-crossing commissural axons exhibited abnormal pathfinding and are defasciculated in the mutant embryos (Figures 5B and 5D, arrowheads). Taken together, our results strongly suggest that Ndfip proteins act *in vivo* to support the timely midline crossing of a significant number of commissural axons.

Because Ndfip1 and Ndfip2 proteins are both capable of downregulating Robo1 *in vitro* and because the single mutants reveal only partial disruption in midline crossing, we next sought to evaluate the consequence of simultaneous removal of both Ndfip1 and Ndfip2. We focused our analysis on E11.5 because at earlier stages (E10.5) Ndfip1 and Ndfip2 single mutants can result in a near complete absence of midline crossing of TAG1-positive axons and to reduce the chance that observed reductions in crossing could be due to developmental delay. As predicted, if Ndfip1 and Ndfip2 work together to promote midline crossing, we find that double mutants have significantly stronger disruptions in midline crossing than Ndfip2 single-mutant sibling controls (Figures 6A–6D). Enhanced crossing defects are observed with both TAG1 and Robo3 antibodies. These observations are consistent with the idea that Ndfip proteins act in parallel to promote midline crossing.

In order to more carefully evaluate the role of Ndfip proteins in the regulation of commissural axon guidance, we performed a series of unilateral dye-labeling experiments to document the behavior of small groups of axons as they approach and cross the midline. E12.5 spinal cords were dissected in open-book preparations from embryos generated by crossing *Ndfip1*$^{+/-}$, *Ndfip2*$^{+/-}$ mice with *Ndfip1*$^{+/-}$, *Ndfip2*$^{-/-}$ mice, and Dil was injected into one side of the dorsal spinal cord. In wild-type controls, the majority of labeled axons at E12.5 have crossed the midline and have turned anteriorly (Figures 6E and 6F). In contrast, labeled axons in Ndfip2$^{-/-}$ spinal cords frequently stop and fail to make the correct anterior turn (Figure 6G). In double-mutant spinal cords, these phenotypes are significantly stronger than those observed in the Ndfip2 single-mutant cords (Figures 6I–6K). In addition, we sometimes observe ipsilateral mis-projections in the spinal cord of Ndfip double mutants (~20% of injection sites) (Figures 6L and 6M). We do not observe these phenotypes in wild-type or single mutants, again suggesting that removing both Ndfip genes results in stronger

axon guidance defects than single mutants. Combined with data from transverse sections of the spinal cord, these observations further support the model that Ndfip1 and Ndfip2 act in parallel to promote the guidance of spinal commissural axons across the midline.

Robo1 Levels Are Increased in *Ndfip1* and *Ndfip2* Mutants

The *Ndfip1* and *Ndfip2* mutant phenotypes in the spinal cord (Figures 5 and S8) are consistent with the idea that some spinal commissural axons fail to cross the floor plate because of elevated expression of Robo, which in turn leads to a premature response to Slit. To test whether the loss of Ndfip1 alters Robo1 levels and localization in commissural axons, we used immunofluorescence to monitor the levels of Robo1 in *Ndfip1* and *Ndfip2* in single- or double-mutant embryos. In wild-type E11.5 embryos, Robo1 is localized primarily to the post-crossing portion of commissural axons, with low levels detected on pre-crossing (Figure 7A, arrows) and crossing commissural axons (Figure 7A, arrowheads). However, in *Ndfip1* mutant embryos, there is a significant elevation of Robo1 levels in pre-crossing commissural axons (Figures 7B and 7C, arrows with asterisks, and Figure 7D) compared with wild-type embryos. There is also a small but significant elevation of Robo1 expression in *Ndfip2* mutants (Figure 7D), and Robo1 expression is further increased in *Ndfip1, Ndfip2* double mutants relative to *Ndfip1* or *Ndfip2* single mutants. Together with our *in vitro* data, these observations suggest that Ndfip proteins promote midline crossing in the mammalian spinal cord by sorting Robo1 for degradation. To further support an *in vivo* role for Ndfip1 in the negative regulation of Robo1 expression, we also examined the levels of Robo1 in *Ndfip1* mutant adult brain and spinal cord extracts. Total Robo1 levels are significantly increased in *Ndfip1* mutant brain and spinal cord compared with wild-type (Figures 7E–7H). This effect is not observed for Robo2, Robo3, or DCC (Figures 7E–7H and S9), indicating the specificity of the effect of Ndfip1 on Robo1 regulation both *in vitro* and *in vivo.* Taken together, our data suggest the existence of functional conservation of Robo1 receptor sorting in flies and mammals to control midline crossing (Figure S10).

DISCUSSION

In this paper, we have described the role of Ndfip proteins in controlling midline crossing through the regulation of Robo1 levels in the mammalian spinal cord. *In vitro* biochemical analyses show that Ndfip1 and Ndfip2 can regulate mammalian Robo1 receptor levels by acting as adaptors to recruit HECT E3 ligases, leading to the ubiquitylation and subsequent degradation of Robo1 via the lysosomal and proteosomal pathways. Loss-of-function and gain-of-function studies demonstrate the specificity of Ndfip proteins in the regulation of the Robo1 receptor. Inhibition of HECT E3 ligases or expression of Ndfip proteins that cannot bind to E3 ligases disrupts the ability of Ndfip proteins to regulate Robo1 surface levels, indicating that the negative regulation of Robo1 requires an active Ndfip-HECT E3 ligase complex. Ndfip proteins are expressed in commissural axons, and in the absence of Ndfip1 or Ndfip2, we observe a significant reduction in midline crossing in the spinal cord and a significant increase in Robo1 expression. Simultaneous removal of Ndfip1 and Ndfip2 in double mutants leads to significantly stronger phenotypes consistent with the idea that the Ndfip proteins act in parallel to regulate spinal commissural axon guidance. Taken together, our results strongly suggest that Ndfip proteins function analogously to Comm to regulate

mammalian Robo1 by recruiting it to endosomes. Furthermore, our biochemical data define an intracellular trafficking pathway consisting of Ndfip adaptor proteins and HECT E3 ubiquitin ligases that act together to promote Robo1 ubiquitylation and its subsequent degradation in lysosomal and proteasomal compartments. We propose that Ndfip/E3 ligase-mediated sorting and degradation of Robo1 in pre-crossing commissural axons in the developing spinal cord ensures midline crossing by preventing the premature response to Slit.

Mammalian Ndfip Proteins Act Analogously to *Drosophila* Comm to Regulate Robo

Several lines of evidence indicate that Comm can recruit the Robo1 receptor directly to endosomes before it reaches the cell surface and that this sorting function is important for controlling axon crossing at the fly embryonic midline (Keleman et al., 2002, 2005). Our results indicate that Ndfip proteins regulate mammalian Robo1 in a Comm-like manner. In support of this, (1) Ndfip proteins can bind to Robo1 and re-localize it to endosomes, (2) overexpression of Ndfip proteins can strongly downregulate Robo1 surface expression, (3) point mutations in the PY motifs in Ndfip proteins prevent the regulation of Robo1 protein levels and localization, (4) Ndfip proteins are expressed in commissural neurons, and (5) *Ndfip1* and *Ndfip2* single mutants result in a failure of some commissural axons to cross the midline and these defects are enhanced in *Ndfip1, Ndfip2* double mutants. It is important to point out that despite an increase in the strength of the midline crossing phenotypes relative to single *Ndfip* mutants, many axons are still able to cross the floor plate in the *Ndfip1, Ndfip2* double mutants. This contrasts with Comm in *Drosophila,* in which mutations in *comm* result in the complete absence of midline crossing in the embryonic CNS. This is perhaps not that surprising given the increased complexity of midline guidance mechanisms and the abundance of molecules that act to normally promote crossing in the mammalian CNS, including Netrin, Shh, VegF, and their respective receptors, as well as Robo3. It would seem that the level of increased Robo repulsion resulting from manipulations to Ndfip proteins is not sufficient to prevent all midline crossing. This could be explained either by the activities of pro-crossing pathways that are unaffected by these manipulations and/or additional mechanisms that act in conjunction with Ndfip-dependent trafficking. Interestingly, a recently published report suggests that an additional mammalian protein, PRRG4, shares some sequence features and *in vitro* properties with *Drosophila comm;* however, the expression and function of this protein in the developing spinal cord have not been investigated (Justice et al., 2017). Taken together, our data suggest the existence of functional conservation of Robo1 receptor sorting in flies and mammals to control midline crossing, despite the fact that the molecules that fulfill this function are not encoded by homologous genes (Figure S10).

Our favored interpretation of the loss-of-function phenotypes in *Ndfip* mutants is that the defects in midline crossing that we observe stem from the elevated expression of Robo1. However, it is possible that the Ndfip defects may be due to effects on other substrate proteins that we have not analyzed. For example, Ndfip proteins could regulate other pathways involved in switching axon responses at the midline. Semaphorin3B-PlexinA1 repulsion is also inhibited before midline crossing, and Plexin protein expression is also regulated during midline crossing (Nawabi et al., 2010). It is also interesting to note that we

actually observe a significant decrease of Robo3 expression in Ndfip1 mutant adult brains relative to control, suggesting a possible indirect link between Ndfip1 and Robo3 in adult brain (Figure S9). Importantly, this reduction in Robo3 expression levels was not observed in the embryonic spinal cord (Figures 5, 6, and S9) or in adult spinal cord extracts (Figure S9). In contrast, Ndfip proteins are sufficient to decrease levels of Robo3 *in vitro* (Figure S1); however, unlike Robo1, we do not observe any increase in Robo3 expression in *Ndfip* mutants in any of the tissues or developmental stages we have examined, suggesting that the regulation of Robo3 by Ndfip proteins may be context specific. A rigorous evaluation of the contribution of the altered levels of Robo1 receptor expression to the *in vivo* mutant phenotypes of Ndfip1 and Ndfip2 will necessitate the generation and analysis of double and triple mutants between Robo1, Ndfip1, and Ndfip2. On the basis of our *in vitro* biochemical data and the expression patterns of Ndfip proteins, we favor the interpretation that Ndfip proteins function cell-autonomously in commissural neurons; however, a rigorous demonstration of this will await the future analysis of conditional removal of Ndfip proteins.

Requirement of E3 Ubiquitin Ligases in the Regulation of the Mammalian Robo1 Receptor

Several guidance receptors are known to be regulated by intracellular trafficking (O'Donnell et al., 2009). For example, Semaphorin3A-induced endocytosis of Neuropilin-1 has been shown to be important for growth cone collapse during axon guidance (Castellani et al., 2004). In *Drosophila,* Comm allows axon growth across the midline by sorting Robo from new membrane vesicles to late endosomes before they can be delivered to the growth cone (Keleman et al., 2002, 2005). It has been proposed that Comm's ability to regulate surface levels of Robo depends on Comm's interaction with and ubiquitylation by the E3 ubiquitin ligase Nedd4 (Myat et al., 2002). However, the observation that a mutant version of Comm that cannot be ubiquitylated can restore Comm's activity and that *Nedd4* zygotic null mutants have no commissural guidance defects *in vivo* argues against the requirement for Nedd4 and Comm ubiquitylation in midline crossing (Keleman et al., 2005). Here we have shown that Ndfip proteins recruit Nedd4-family E3 ubiquitin ligases that ubiquitylate Robo1 receptors and lead to their subsequent proteosomal and lysosomal degradation. Whether Comm also recruits E3 ligases to drive the ubiquitylation and degradation of *Drosophila* Robo receptors remains to be tested. Given that multiple studies have demonstrated that in addition to regulating Robo localization, Comm also negatively regulates Robo protein levels (Gilestro, 2008; Kidd et al., 1998; Myat et al., 2002), it is surprising that the ubiquitylation of the *Drosophila* Robo receptor has not been investigated. It is worth noting here that in addition to Nedd4, there are two other Nedd4 family members in *Drosophila:* Suppressor of deltex (Su[dx]) and dSmurf (Dalton et al., 2011); thus, whether E3 ubiquitin ligase activity is required in *Drosophila* for the regulation of Robo during midline crossing is still an open question.

In mammals, the Nedd4 family has further expanded and includes Nedd4 (Nedd4-1), Nedd4L (Nedd4-2), Itch, WWP1, WWP2, Smurf1, Smurf2, NEDL1, and NEDL2 (Ingham et al., 2004; Rotin and Kumar, 2009). Nedd4 is a positive regulator of cell proliferation and animal growth. *Nedd4* mutant mice are small, and *Nedd4* mutant mouse embryonic fibroblasts (MEFs) have less mitogenic activity (Cao et al., 2008; Fouladkou et al., 2008). SMURFs have a major role in the regulation of TGF beta signaling (Massagué and Gomis,

2006), whereas ITCH regulates the immune system by controlling the levels of its substrate, JUNB (Gao et al., 2004). Recent evidence also suggests that Nedd4-family E3 ligases promote axonal growth and branching in the developing mammalian brain (Hsia et al., 2014). Interestingly, several of these Nedd4 ligases are strongly expressed in the post-natal mouse spinal cord (The Allen Brain Atlas [http://mousespinal.brain-map.org/]).

Ndfip1 and Ndfip2 are a subset of proteins that interact with Nedd4 E3 ligases to modulate their enzymatic activity and substrate binding (Mund and Pelham, 2009; Riling et al., 2015). Ndfip proteins act as adaptors for Itch to regulate T cell activation (Oliver et al., 2006), and they are also required for WWP2 to regulate iron homeostasis through DMT1 (Foot et al., 2008). Although our *in vitro* biochemical data using Ndfip proteins with mutations in their PY motifs and the HECT E3 ligase inhibitor Heclin strongly suggest the involvement of Nedd4 ligases in the regulation of mammalian Robo1 levels and axon guidance *in vivo,* the requirement for and identity of the specific Nedd4-family E3 ligases await future investigation.

How Is the Expression of Ndfip1 and Ndfip2 Regulated in the Developing Spinal Cord?

Our *in vivo* expression data that Ndfip1 is specifically expressed in commissural axons that are crossing the midline suggest that it may promote their crossing by decreasing Robo1. How is this spatial expression of Ndfip regulated? In *Drosophila,* Comm expression is regulated partly by Fra, the *Drosophila* ortholog of the DCC receptor. The intracellular domain of Fra is released by γ-secretase proteolysis and functions as a transcriptional activator to induce *Comm* transcription (Neuhaus-Follini and Bashaw, 2015b). Interestingly, DCC is also proteolytically processed, and its intracellular domain can enter the nucleus to regulate gene expression *in vitro* (Bai et al., 2011; Taniguchi et al., 2003). It will be interesting to determine if DCC has a role in the transcriptional regulation of Ndfip1 and/or Ndfip2 during the development of the spinal cord.

In addition to potential transcriptional regulation, the levels of Ndfip proteins are known to be regulated post-translationally through ubiquitylation mediated by Nedd4-family proteins (Harvey et al., 2002; Shearwin-Whyatt et al., 2004). In this regard, it is interesting to note that mutating the PY motifs of Ndfip1 has a profound stabilizing effect on the Ndfip1 protein itself, consistent with previous reports that Ndfip1 is itself a target for E3-ligase dependent degradation (see Figures S4 and 3F). This stabilizing effect of the PY mutations is much more pronounced for Ndfip1 than Ndfip2. The possibility that Ndfip1 could be ubiquitylated and degraded together with its substrate would also be consistent with a role in the transient downregulation of Robo1. Finally, another post-translational modification, phosphorylation, may also have a role in controlling Ndfip expression of activity, as it has been shown that Ndfip proteins undergo EGFR dependent tyrosine phosphorylation (Mund and Pelham, 2010).

Robo, Ndfip, and Nedd4 Family Proteins in Developmental Disorders

Disruption of Slit-Robo signaling and altered regulation of axon guidance receptor levels more generally are implicated in autism spectrum disorders (ASDs) and in movement disorders (Blockus and Chédotal, 2014; Jen et al., 2004; Suda et al., 2011). Interestingly,

mutations in genes encoding HECT E3 ligases have been characterized in patients with severe intellectual disability and ASDs (Ambrozkiewicz and Kawabe, 2015). Thus, further investigation of the molecular function of Ndfip proteins and HECT E3 ligases in the regulation of Slit-Robo signaling in the developing and adult nervous system may provide new insights in the pathophysiology of diverse developmental disorders.

STAR★METHODS

CONTACT FOR REAGENT AND RESOURCE SHARING

Further information and requests for resources and reagents should be directed to the Lead Contact, Greg J. Bashaw (gbashaw@pennmedicine.upenn.edu).

EXPERIMENTAL MODELS AND SUBJECT DETAILS

Mice—Mice were maintained in a barrier facility at the University of Pennsylvania. All mouse work was approved by the Institutional Care and Use Committee of the University of Pennsylvania. Both male and female mouse embryos were used in this study.

Tissue Cell Culture—COS-7, 293T and HeLa cells were maintained in DMEM, supplemented with 10% (vol/vol) FBS and a mixture of 1% penicillin and streptomycin (P/S) at 37°C in a humidified 5% CO_2 incubator.

Primary Neuron Cultures—Commissural neurons from wild-type E12.5 mouse embryonic dorsal spinal cord were prepared as described (Langlois et al., 2010). Dissociated dorsal spinal commissural neurons pooled from both sexes were plated on poly-L-lysine and laminin coated coverslips at low density. Neurons were cultured in neurobasal medium supplemented with 1x B27, 1x Pen/Strep, 1x glutamine and 35 mM glucose.

METHOD DETAILS

Mouse strains and genotyping—Embryos were derived from timed matings with *Ndfip1*−/− *Rag1*−/− male and *Ndfip1*+/− *Rag1*+/+ female mice. Ndfip2 mutant embryos were derived from timed matings with *Ndfip2*−/− male and *Ndfip2*−/− female mice. To obtain Ndfip2 control embryos, timed matings were performed with *Ndfip2*−/− male and wild-type C57BL/6 female mice. *Ndfip1* and *Ndfip2* double mutant embryos were derived from timed matings with *Ndfip1*+/−;*Ndfip2*+/− male with either *Ndfip1*+/−;*Ndfip2*+/− or *Ndfip1*+/−;*Ndfip2*−/− female mice. The day of the vaginal plug was counted as embryonic day 0.5 (E0.5), and embryos were harvested at the indicated embryonic stage. Genotypes were determined by PCR using genomic DNA extracted from embryonic tail. *Ndfip1* WT/KO embryos were genotyped by PCR using the following primers: Ndfip1 WT Forward: 5′ TAGGCCAAGGTGAAAACTGG 3′; Ndfip1 WT Reverse: 5′ AGAGGTGGGTTCAACAGTGG 3′. Ndfip1 KO Forward: 5′ CGACTTCCAGTTCAACATCAGC 3′; Ndfip1 KO Reverse: 5′ GTCTGTTGTGCCCAGTCATAGC 3′. Ndfip2 KO/KI embryos were genotyped by PCR using the following primers: Ndfip2 WT Forward: 5′ CCCTGTGCCACCTCCGTACAGTG 3′; Ndfip2 WT Reverse: 5′ GCTGAGGCAGTGCGCAGACTTAC 3′; Ndfip2 KO/KI Forward: 5′ CTTCAAGCAGACCTACAGCAAG 3′; Ndfip2 KO/KI Reverse: 5′

CCTGTTATCCCTAGCGTAACG 3′. For the western blot analysis for Figures 7E and S9A, brain extracts were prepared from age-matched *Rag1*−/− and *Ndfip1*−/− *Rag1*−/− adult mice. For the western blot analysis for Figures 7F and S9B, spinal cord extracts were obtained from age-matched *Ndfip1*+/+ and *Ndfip1*−/− adult mice.

Cell Transfections—COS-7, 293T and HeLa cells were transiently transfected with Effectene transfection reagent (QIAGEN, Valencia CA). All transfections were carried out according to the manufacturer's instructions.

Immunofluorescence Experiments—Dissociated dorsal spinal commissural neurons and transiently transfected COS-7 cells were washed once with ice-cold PBS, fixed for 15 min in 4% paraformaldehyde at room temperature, permeabilized with 0.1% Triton X-100 in PBS (PBT) for 10 min and then blocked in PBT + 5% NGS (normal goat serum) for 30 min at room temperature. Cells were then incubated with primary antibodies diluted in PBT + 5% NGS overnight at 4°C. After three washes in PBT, secondary antibodies diluted in PBT + 5% NGS were added and incubated for 1h at room temperature. After secondary antibodies, cells were washed three times in PBS and coverslips were mounted in Aquamount. For surface labeling in transiently transfected COS-7 cells, cells were washed with ice-cold PBS and blocked in PBS + 5% NGS for 20 min at 4°C. Cells were then incubated in primary antibodies diluted in PBS + 5% NGS for 30 min at 4°C, then washed three times in cold PBS. Cells were fixed for 15 min at 4°C in 4% paraformaldehyde in PBS, followed by three washes in PBS and stained with other primary antibodies diluted in PBT + 5% NGS overnight at 4°C. After three washes in PBS, cells were incubated with secondary antibodies diluted in PBT + 5% NGS for 30 min at room temperature. Antibodies used: Rabbit anti-Myc (1:500, Sigma, C3956-2MG), mouse anti-HA (1:1000, BioLegend # 901502), rabbit anti-Ndfip1 (1:100, Sigma #HPA009682), mouse anti-TAG1 (1:100, DSHB#4D7), Cy3 goat anti-mouse (1:1000, Jackson Immunoresearch #115-165-003), and Alexa488 goat anti-rabbit (Invitrogen, 1:500 #A11034).

Cell-surface biotinylation—Cell surface biotinylation experiments were performed as follows. Briefly, 48 hours after transfection, HeLa cells were washed twice with ice-cold $DPBS^+$ and incubated with 2.5 mg/ml EZ-link Sulfo-NHS-LC-LC-biotin reagent for 30 min on ice with gentle rocking. Biotinylation was performed at 4°C to ensure that the coupling reaction would only take place on surface proteins and that no activated biotin could be internalized. After incubation, cells were washed three times with ice-cold 100 mM Glycine in $DPBS^+$, followed with ice-cold 20 mM Glycine in $DPBS^+$ at 4°C. Cells were then lysed in buffer containing 150 mM NaCl, 50 mM Tris pH-7.4, 1 mM EDTA supplemented with 0.5% Surfact-AMPS NP40 (Thermo, Waltham MA), Complete Protease Inhibitor (Roche), and 1 mM phenylmethanesulfonylfluoride (PMSF) for 1hr on ice. Supernatants were collected after centrifugation at 16,000 x g for 15 minutes at 4°C. 10%–15% of supernatant was transferred into another tube, which was used as a total lysate/input. $DPBS^+$ washed NeutrAvidin Ultralink beads (Thermo Scientific #53150) were added to the remaining supernatant and incubated overnight on a nutator at 4°C. After incubation, beads were washed three times with lysis buffer and boiled for 10 min in 2x Laemmli SDS sample buffer and analyzed by western blotting with anti-Myc antibody to detect the surface protein.

Antibodies used: mouse anti-myc (1:1000, 9E10-c, DHSB), mouse anti-HA (1:1000, BioLegend # 901502), mouse anti-beta tubulin (1:1000, E7, DSHB), and goat anti-mouse HRP (1:10,000, Jackson Immunoresearch#115-035-146).

Immunoprecipitation—48 hours after transient transfections, cells were washed in PBS and subsequently lysed in TBS supplemented with 1% Triton X-100 (EMD Millipore), Complete Protease Inhibitor (Roche), and 1 mM PMSF for 30 min on a nutator at 4°C. Soluble proteins were recovered by centrifugation at 15,000 x g for 15 min at 4°C. Lysates were incubated with 1–2 μg of antibody overnight on a nutator at 4°C. After incubation, 50 μL of a 50% slurry of protein A and proteinG agarose (Invitrogen) were added, and samples were incubated for an additional 2 hr with gentle rocking at 4°C. The immunocomplexes were washed three times with wash buffer (TBS with 0.1% Triton X-100) and boiled for 10 min in 2x Laemmli SDS sample buffer and analyzed by western blotting. Proteins were resolved by SDS-PAGE and transferred to nitrocellulose membranes (Amersham, UK). Membranes were blocked with 5% dry milk and 0.1% Tween 20 in PBS for 1 hr at room temperature and incubated with primary antibodies overnight at 4°C. After three washes in PBS/0.1% Tween 20, membranes were incubated with the appropriate HRP-conjugated secondary antibody at room temperature for 1h. Signals were detected using ECL Prime (Amersham, UK) according to manufacturer's instructions. Antibodies used: for immunoprecipitation, rabbit anti-Myc (1:200, Millipore #06-549), and for western blot, mouse anti-FLAG (1:1000, Sigma, F1804-50UG), mouse anti-HA (1:1000, BioLegend #901502), mouse anti-myc (1:1000, 9E10, DSHB), mouse anti-beta tubulin (1:1000, E7, DSHB), rabbit anti-integrinβ1 (1:1000, Cell Signaling Technology #4706S), goat anti-rabbit HRP (1:10,000, Jackson Immunoresearch #111-035-003) and goat anti-mouse HRP (1:10,000, Jackson Immunoresearch #115-035-146).

For preparation of mouse brain and spinal cord lysates, wild-type and *Ndfip1* KO mice were anesthetized and whole brain and spinal cord were dissected and lysed in TBS supplemented with 1% Triton X-100, Complete Protease Inhibitor, and 1 mM PMSF by using a dounce homogenizer. Homogenized samples were incubated on ice for 1 hr and centrifuged at 16,000 x g in an ice-cold centrifuge. Supernatants were collected after centrifugation and immunoprecipitation and western blotting were performed as described above. Antibodies used: mouse anti-Ndfip1 (D-4) (1:50, Santa Cruz Biotechnology #sc-398469), mouse anti-Ndfip2 (E-4) (1:50, Santa Cruz Biotechnology #sc-376259), goat anti-Robo1 (1:500, R&D systems #AF1749), goat anti-Robo2 (1:500, R&D systems #AF3147), goat anti-Robo3 (1:1000, R&D systems #AF3076), goat anti-DCC (1:500, R&D systems #AF844) and donkey anti-goat HRP (1:10,000, Jackson Immunoresearch #705-035-003).

Immunohistochemistry—Embryos were fixed in 4% paraformaldehyde (Sigma) in PBS for 2 h at 4°C, cryoprotected in 30% sucrose in PBS overnight and frozen in NEG-50 Frozen Section Medium (Thermo Fisher). Frozen embryos were thin-sectioned to yield 20 μM transverse sections with a cryostat. Antibody staining was performed on cryostat sections after blocking in 5% NGS in PBS containing 0.1% Triton X-100 or with 2% horse serum in PBS containing 0.1% Triton X-100 (for all anti-goat antibodies) for 1h at room temperature. Sections were then incubated with primary antibodies overnight at 4°C. After three washes

in PBS, sections were incubated with species-specific secondary antibodies conjugated to fluorophores at room temperature for 2 hr. Antibodies used: rabbit anti-Ndfip1 (1:100, Sigma #HPA009682), mouse anti-TAG1 (1:100, DSHB #4D7), goat anti-Robo3 (1:200, R&D systems #AF3076), goat anti-Robo1 (1:200, R&D systems #AF1749), rabbit anti-GFP (1:1000, Invitrogen #A11122), rat anti-L1CAM (1:300, Millipore #MAB5272), Alexa488 goat anti-rabbit (Invitrogen, 1:500 #A11034), Cy3 goat anti-mouse (1:1000, Jackson Immunoresearch # 115-165-003), Cy3 donkey anti-goat (1:400, Jackson Immunoresearch #705-165-003), and Alexa633 goat anti-Rat (1:500, Invitrogen #A-21094).

***In situ* hybridization—**DIG-labeled riboprobes were synthesized using a DIG RNA labeling kit (Roche) and were used on 20μm transverse sections. Template for Ndfip1 probe was amplified from a mouse DRG cDNA library and Ndfip2 probe was amplified from mouse Ndfip2 ORF clone (Origene #MR202968). mRNA signal was visualized using BCIP/NBT and AP-conjugated anti-DIG antibody. Primers used to amplify cDNA were: Ndfip1 (5′- AGAACGTCTCAGCGTCGG –3′ and 5′-CAGGAAGCCTTTGCCAGA –3′) and Ndfip2 (5′-ATGCGCGTCCGCGCCGAGCAT –3′ and 5′-CTCGTCCTATGTGCAGCCGCCATAC –3′).

Open-book spinal cord preparations and Dye injections—Open book preparation from E12.5 spinal cords were isolated as previously described (Lyuksyutova et al., 2003). After dissecting open-books, we fixed open-book preparations in 4% PFA for 45 - 60 min in 4°C. After fixation, open-books were incubated in ice-cold PBS until ready to inject with Dil. We made multiple injections in the dorsal spinal cord cell bodies with Fast Dil (5 mg/ml Dil in DMSO) using a very fine needle. Leaked Dil was removed by washing open-books in ice cold PBS. Dil injected open-book preparations were incubated in ice cold PBS at 4°C for 3 days to let the dye to diffuse.

QUANTIFICATION AND STATISTICAL ANALYSIS

Embryos were scored blind to genotype. Data are presented as mean values ± s.e.m. All statistical analyses were performed using the Student’s t test. All statistics and graphs were generated using Microsoft Excel. Differences were considered significant when $p < 0.05$. The thickness of spinal commissural bundle was quantified for each embryo on five to eight sections per embryo. Three to four embryos of each genotype were quantified. The ratio of the commissural axon bundle size was normalized to wild-type or heterozygous sibling controls. In order to control for any variability in the size of embryo, the values of commissure thickness were normalized with length of spinal cord. For western blots, densitometry analysis was performed and quantified from three independent experiments and normalized with tubulin levels. For surface labeling, fluorescence intensity was measured as mean gray value (integrated density/area) by drawing an outer and inner rings on either side of cell surface using ImageJ.

Supplementary Material

Refer to Web version on PubMed Central for supplementary material.

ACKNOWLEDGMENTS

We would like to acknowledge Wenqin Luo, Kim Kridsada, other members of the Luo lab, and Elise Arbeille for help in preparation of mouse tissue for sectioning and advice on spinal cord anatomy and imaging. We thank Thomas Mund and Hugh Pellham for the gift of Ndfip plasmids. We thank Hideaki Fujita for the gift of FLAG-UB plasmid and Weining Lu for the gift of hRobo2 construct. We thank Alain Chédotal for the gift of mRobo3.1A-Myc construct. We also thank members of the Bashaw lab for constructive comments during the course of this work and Alexandra Neuhaus-Follini, Samantha Butler, and Lisa Goodrich for critical comments on the manuscript. Grants to G.J.B. from the NSF (IOS-1355181) and NIH (R35 NS097340) supported this research.

REFERENCES

Ambrozkiewicz MC, and Kawabe H (2015). HECT-type E3 ubiquitin ligases in nerve cell development and synapse physiology. FEBS Lett 589, 1635–1643. [PubMed: 25979171]

Bai G, Chivatakarn O, Bonanomi D, Lettieri K, Franco L, Xia C, Stein E, Ma L, Lewcock JW, and Pfaff SL (2011). Presenilin-dependent receptor processing is required for axon guidance. Cell 144, 106–118. [PubMed: 21215373]

Blockus H, and Chédotal A (2014). The multifaceted roles of Slits and Robos in cortical circuits: from proliferation to axon guidance and neurological diseases. Curr. Opin. Neurobiol 27, 82–88. [PubMed: 24698714]

Brose K, Bland KS, Wang KH, Arnott D, Henzel W, Goodman CS, Tessier-Lavigne M, and Kidd T (1999). Slit proteins bind Robo receptors and have an evolutionarily conserved role in repulsive axon guidance. Cell 96, 795–806. [PubMed: 10102268]

Cao XR, Lill NL, Boase N, Shi PP, Croucher DR, Shan H, Qu J, Sweezer EM, Place T, Kirby PA, et al. (2008). Nedd4 controls animal growth by regulating IGF-1 signaling. Sci. Signal 1, ra5. [PubMed: 18812566]

Castellani V, Falk J, and Rougon G (2004). Semaphorin3A-induced receptor endocytosis during axon guidance responses is mediated by L1 CAM. Mol. Cell. Neurosci 26, 89–100. [PubMed: 15121181]

Charron F, Stein E, Jeong J, McMahon AP, and Tessier-Lavigne M (2003). The morphogen sonic hedgehog is an axonal chemoattractant that collaborates with netrin-1 in midline axon guidance. Cell 113, 11–23. [PubMed: 12679031]

Dalton HE, Denton D, Foot NJ, Ho K, Mills K, Brou C, and Kumar S (2011). Drosophila Ndfip is a novel regulator of Notch signaling. Cell Death Differ 18, 1150–1160. [PubMed: 20966964]

Dickson BJ, and Zou Y (2010). Navigating intermediate targets: the nervous system midline. Cold Spring Harb. Perspect. Biol 2, a002055. [PubMed: 20534708]

Engle EC (2010). Human genetic disorders of axon guidance. Cold Spring Harb. Perspect. Biol 2, a001784. [PubMed: 20300212]

Evans TA, and Bashaw GJ (2010). Axon guidance at the midline: of mice and flies. Curr. Opin. Neurobiol 20, 79–85. [PubMed: 20074930]

Evans TA, and Bashaw GJ (2012). Slit/Robo-mediated axon guidance in Tribolium and Drosophila: divergent genetic programs build insect nervous systems. Dev. Biol 363, 266–278. [PubMed: 22245052]

Evans TA, Santiago C, Arbeille E, and Bashaw GJ (2015). Robo2 acts in trans to inhibit Slit-Robo1 repulsion in pre-crossing commissural axons. ELife 4, e08407. [PubMed: 26186094]

Foot NJ, Dalton HE, Shearwin-Whyatt LM, Dorstyn L, Tan SS, Yang B, and Kumar S (2008). Regulation of the divalent metal ion transporter DMT1 and iron homeostasis by a ubiquitin-dependent mechanism involving Ndfips and WWP2. Blood 112, 4268–4275. [PubMed: 18776082]

Fouladkou F, Landry T, Kawabe H, Neeb A, Lu C, Brose N, Stambolic V, and Rotin D (2008). The ubiquitin ligase Nedd4-1 is dispensable for the regulation of PTEN stability and localization. Proc. Natl. Acad. Sci. U S A 105, 8585–8590. [PubMed: 18562292]

Gao M, Labuda T, Xia Y, Gallagher E, Fang D, Liu YC, and Karin M (2004). Jun turnover is controlled through JNK-dependent phosphorylation of the E3 ligase Itch. Science 306, 271–275. [PubMed: 15358865]

Gilestro GF (2008). Redundant mechanisms for regulation of midline crossing in Drosophila. PLoS ONE 3, e3798. [PubMed: 19030109]

Goh CP, Low LH, Putz U, Gunnersen J, Hammond V, Howitt J, and Tan SS (2013). Ndfip1 expression in developing neurons indicates a role for protein ubiquitination by Nedd4 E3 ligases during cortical development. Neurosci. Lett 555, 225–230. [PubMed: 24036464]

Hammond VE, Gunnersen JM, Goh CP, Low LH, Hyakumura T, Tang MM, Britto JM, Putz U, Howitt JA, and Tan SS (2014). Ndfip1 is required for the development of pyramidal neuron dendrites and spines in the neocortex. Cereb. Cortex 24, 3289–3300. [PubMed: 23897647]

Harvey KF, Shearwin-Whyatt LM, Fotia A, Parton RG, and Kumar S (2002). N4WBP5, a potential target for ubiquitination by the Nedd4 family of proteins, is a novel Golgi-associated protein. J. Biol. Chem 277, 9307–9317. [PubMed: 11748237]

Howitt J, Lackovic J, Low LH, Naguib A, Macintyre A, Goh CP, Callaway JK, Hammond V, Thomas T, Dixon M, et al. (2012). Ndfip1 regulates nuclear Pten import in vivo to promote neuronal survival following cerebral ischemia. J. Cell Biol 196, 29–36. [PubMed: 22213801]

Hsia HE, Kumar R, Luca R, Takeda M, Courchet J, Nakashima J, Wu S, Goebbels S, An W, Eickholt BJ, et al. (2014). Ubiquitin E3 ligase Nedd4-1 acts as a downstream target of PI3K/PTEN-mTORC1 signaling to promote neurite growth. Proc. Natl. Acad. Sci. U S A 111, 13205–13210. [PubMed: 25157163]

Ingham RJ, Gish G, and Pawson T (2004). The Nedd4 family of E3 ubiquitin ligases: functional diversity within a common modular architecture. Oncogene 23, 1972–1984. [PubMed: 15021885]

Ishii N, Wadsworth WG, Stern BD, Culotti JG, and Hedgecock EM (1992). UNC-6, a laminin-related protein, guides cell and pioneer axon migrations in C. elegans. Neuron 9, 873–881. [PubMed: 1329863]

Jamuar SS, Schmitz-Abe K, D'Gama AM, Drottar M, Chan WM, Peeva M, Servattalab S, Lam AN, Delgado MR, Clegg NJ, et al. (2017). Biallelic mutations in human DCC cause developmental split-brain syndrome. Nat. Genet 49, 606–612. [PubMed: 28250456]

Jen JC, Chan WM, Bosley TM, Wan J, Carr JR, Rüb U, Shattuck D, Salamon G, Kudo LC, Ou J, et al. (2004). Mutations in a human ROBO gene disrupt hindbrain axon pathway crossing and morphogenesis. Science 304, 1509–1513. [PubMed: 15105459]

Justice ED, Barnum SJ, and Kidd T (2017). The WAGR syndrome gene PRRG4 is a functional homologue of the commissureless axon guidance gene. PLoS Genet 13, e1006865. [PubMed: 28859078]

Keleman K, Rajagopalan S, Cleppien D, Teis D, Paiha K, Huber LA, Technau GM, and Dickson BJ (2002). Comm sorts robo to control axon guidance at the Drosophila midline. Cell 110, 415–427. [PubMed: 12202032]

Keleman K, Ribeiro C, and Dickson BJ (2005). Comm function in commissural axon guidance: cell-autonomous sorting of Robo in vivo. Nat. Neurosci 8, 156–163. [PubMed: 15657595]

Kidd T, Russell C, Goodman CS, and Tear G (1998). Dosage-sensitive and complementary functions of roundabout and commissureless control axon crossing of the CNS midline. Neuron 20, 25–33. [PubMed: 9459439]

Kidd T, Bland KS, and Goodman CS (1999). Slit is the midline repellent for the robo receptor in Drosophila. Cell 96, 785–794. [PubMed: 10102267]

Langlois SD, Morin S, Yam PT, and Charron F (2010). Dissection and culture of commissural neurons from embryonic spinal cord. J. Vis. Exp (39), 1773. [PubMed: 20505653]

Layman AAK, Sprout SL, Phillips D, and Oliver PM (2017). Ndfip1 restricts Th17 cell potency by limiting lineage stability and proinflammatory cytokine production. Sci. Rep 7, 39649. [PubMed: 28051111]

Lyuksyutova AI, Lu CC, Milanesio N, King LA, Guo N, Wang Y, Nathans J, Tessier-Lavigne M, and Zou Y (2003). Anterior-posterior guidance of commissural axons by Wnt-frizzled signaling. Science 302, 1984–1988. [PubMed: 14671310]

Massagué J, and Gomis RR (2006). The logic of TGFbeta signaling. FEBS Lett 580, 2811–2820. [PubMed: 16678165]

Mitchell KJ, Doyle JL, Serafini T, Kennedy TE, Tessier-Lavigne M, Goodman CS, and Dickson BJ (1996). Genetic analysis of Netrin genes in Drosophila: Netrins guide CNS commissural axons and peripheral motor axons. Neuron 17, 203–215. [PubMed: 8780645]

Mund T, and Pelham HR (2009). Control of the activity of WW-HECT domain E3 ubiquitin ligases by NDFIP proteins. EMBO Rep 10, 501–507. [PubMed: 19343052]

Mund T, and Pelham HR (2010). Regulation of PTEN/Akt and MAP kinase signaling pathways by the ubiquitin ligase activators Ndfip1 and Ndfip2. Proc. Natl. Acad. Sci. U S A 107, 11429–11434. [PubMed: 20534535]

Mund T, Lewis MJ, Maslen S, and Pelham HR (2014). Peptide and small molecule inhibitors of HECT-type ubiquitin ligases. Proc. Natl. Acad. Sci. U S A 111, 16736–16741. [PubMed: 25385595]

Myat A, Henry P, McCabe V, Flintoft L, Rotin D, and Tear G (2002). Drosophila Nedd4, a ubiquitin ligase, is recruited by Commissureless to control cell surface levels of the roundabout receptor. Neuron 35, 447–459. [PubMed: 12165468]

Nawabi H, Briançon-Marjollet A, Clark C, Sanyas I, Takamatsu H, Okuno T, Kumanogoh A, Bozon M, Takeshima K, Yoshida Y, et al. (2010). A midline switch of receptor processing regulates commissural axon guidance in vertebrates. Genes Dev 24, 396–410. [PubMed: 20159958]

Neuhaus-Follini A, and Bashaw GJ (2015a). Crossing the embryonic midline: molecular mechanisms regulating axon responsiveness at an intermediate target. Wiley Interdiscip. Rev. Dev. Biol 4, 377–389. [PubMed: 25779002]

Neuhaus-Follini A, and Bashaw GJ (2015b). The intracellular domain of the Frazzled/DCC receptor is a transcription factor required for commissural axon guidance. Neuron 87, 751–763. [PubMed: 26291159]

O'Donnell M, Chance RK, and Bashaw GJ (2009). Axon growth and guidance: receptor regulation and signal transduction. Annu. Rev. Neurosci 32, 383–412. [PubMed: 19400716]

O'Leary CE, Riling CR, Spruce LA, Ding H, Kumar S, Deng G, Liu Y, Seeholzer SH, and Oliver PM (2016). Ndfip-mediated degradation of Jak1 tunes cytokine signalling to limit expansion of CD4+ effector T cells. Nat. Commun 7, 11226. [PubMed: 27088444]

Oliver PM, Cao X, Worthen GS, Shi P, Briones N, MacLeod M, White J, Kirby P, Kappler J, Marrack P, and Yang B (2006). Ndfip1 protein promotes the function of itch ubiquitin ligase to prevent T cell activation and T helper 2 cell-mediated inflammation. Immunity 25, 929–940. [PubMed: 17137798]

Ramon HE, Beal AM, Liu Y, Worthen GS, and Oliver PM (2012). The E3 ubiquitin ligase adaptor Ndfip1 regulates Th17 differentiation by limiting the production of proinflammatory cytokines. J. Immunol 188, 4023–4031. [PubMed: 22403444]

Riling C, Kamadurai H, Kumar S, O'Leary CE, Wu KP, Manion EE, Ying M, Schulman BA, and Oliver PM (2015). Itch WW domains inhibit its E3 ubiquitin ligase activity by blocking E2-E3 ligase trans-thiolation. J. Biol. Chem 290, 23875–23887. [PubMed: 26245901]

Rotin D, and Kumar S (2009). Physiological functions of the HECT family of ubiquitin ligases. Nat. Rev. Mol. Cell Biol 10, 398–409. [PubMed: 19436320]

Sabatier C, Plump AS, Le Ma, Brose K, Tamada A, Murakami F, Lee EY, and Tessier-Lavigne M (2004). The divergent Robo family protein rig-1/Robo3 is a negative regulator of slit responsiveness required for midline crossing by commissural axons. Cell 117, 157–169. [PubMed: 15084255]

Serafini T, Colamarino SA, Leonardo ED, Wang H, Beddington R, Skarnes WC, and Tessier-Lavigne M (1996). Netrin-1 is required for commissural axon guidance in the developing vertebrate nervous system. Cell 87, 1001–1014. [PubMed: 8978605]

Shearwin-Whyatt LM, Brown DL, Wylie FG, Stow JL, and Kumar S (2004). N4WBP5A (Ndfip2), a Nedd4-interacting protein, localizes to multivesicular bodies and the Golgi, and has a potential role in protein trafficking. J. Cell Sci 117, 3679–3689. [PubMed: 15252135]

Suda S, Iwata K, Shimmura C, Kameno Y, Anitha A, Thanseem I, Nakamura K, Matsuzaki H, Tsuchiya KJ, Sugihara G, et al. (2011). Decreased expression of axon-guidance receptors in the anterior cingulate cortex in autism. Mol. Autism 2, 14. [PubMed: 21859478]

Taniguchi Y, Kim SH, and Sisodia SS (2003). Presenilin-dependent "gamma-secretase" processing of deleted in colorectal cancer (DCC). J. Biol. Chem 278, 30425–30428. [PubMed: 12840034]

Tear G, Harris R, Sutaria S, Kilomanski K, Goodman CS, and Seeger MA (1996). commissureless controls growth cone guidance across the CNS midline in Drosophila and encodes a novel membrane protein. Neuron 16, 501–514. [PubMed: 8785048]

Vallstedt A, and Kullander K (2013). Dorsally derived spinal interneurons in locomotor circuits. Ann. N Y Acad. Sci 1279, 32–42. [PubMed: 23531000]

Yang L, Garbe DS, and Bashaw GJ (2009). A frazzled/DCC-dependent transcriptional switch regulates midline axon guidance. Science 324, 944–947. [PubMed: 19325078]

Zelina P, Blockus H, Zagar Y, Péres A, Friocourt F, Wu Z, Rama N, Fouquet C, Hohenester E, Tessier-Lavigne M, et al. (2014). Signaling switch of the axon guidance receptor Robo3 during vertebrate evolution. Neuron 84, 1258–1272. [PubMed: 25433640]

Zou Y, Stoeckli E, Chen H, and Tessier-Lavigne M (2000). Squeezing axons out of the gray matter: a role for slit and semaphorin proteins from midline and ventral spinal cord. Cell 102, 363–375. [PubMed: 10975526]

Highlights

- Ndfip proteins bind to and recruit the Robo1 receptor to late endosomes
- Ndfip proteins recruit Nedd4-family E3 ubiquitin ligases to trigger Robo degradation
- Loss of Ndfip proteins results in a significant reduction of midline crossing
- Robo1 expression on pre-crossing commissural axons is increased in Ndfip mutants

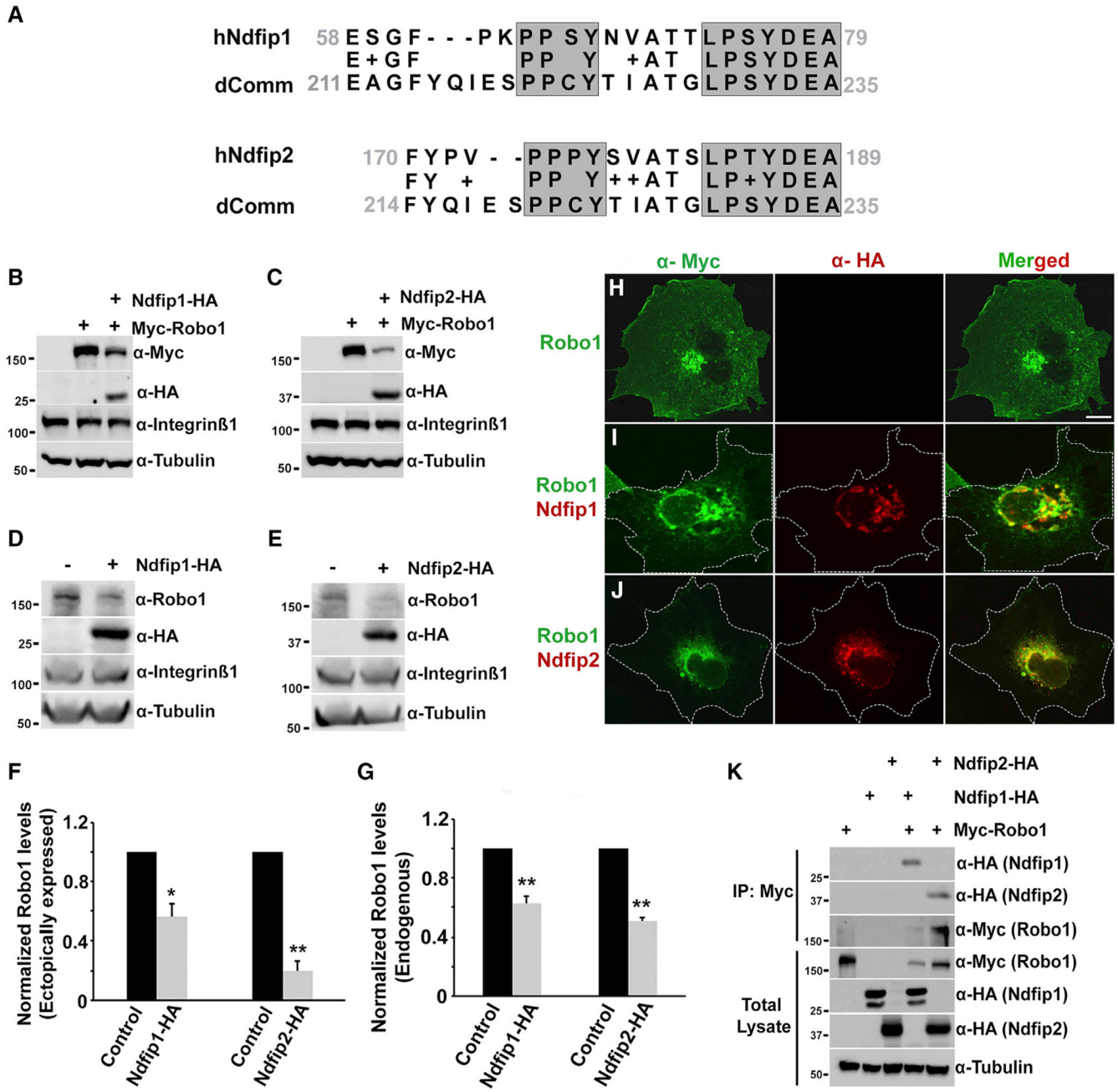

Figure 1. Ndfip1 and Ndfip2 Trigger Robo1 Re-localization and Degradation *In Vitro*

(A) Sequence alignment showing the conservation of the PY (PPxY and LPxY) motifs between *Drosophila* Comm and mammalian Ndfip proteins.

(B and C) Cos-7 cells were transiently co-transfected with Myc-Robo1 (0.5 μg) and with N-terminally HA-tagged Ndfip1 (B) or Ndfip2 (C) (0.5 μg) expression constructs. 48 h after transfection, cell extracts were prepared and analyzed using western blotting with anti-Myc and anti-HA antibodies. Robo1 levels are strongly reduced in cells transfected with either Ndfip1 or Ndfip2 (Ndfip1: 0.56 ± 0.09, p = 0.013; Ndfip2: 0.194 ± 0.06, p = 0.002).

(D and E) HeLa cells were transiently transfected with either HA-tagged Ndfip1 (D) or Ndfip2 (E) (0.5 μg) expression constructs, and the levels of endogenous Robo1 protein were analyzed using anti-Robo1 antibody. Endogenous Robo1 levels were reduced in both Ndfip1- and Ndfip2-transfected cells (Ndfip1: 0.62 ± 0.04, $p = 0.005$; Ndfip2: 0.50 ± 0.02, $p = 0.0009$), but integrin beta-1 receptor levels are unaltered. An anti-Tubulin antibody was used to control for equal protein loading.

(F and G) Quantitative representations of band intensities of Myc-tagged Robo1 (F) or endogenous Robo1 (G) levels in Ndfip1- and Ndfip2-transfected cells.

(H–J) Confocal micrographs of COS-7 cells expressing Myc-tagged Robo1 and HA-tagged Ndfip1 or Ndfip2.

(H) In cells that were transfected with Myc-Robo1 alone, Robo1 was mainly at the plasma membrane and Golgi apparatus.

(I and J) Co-transfection of Myc-Robo1 (in green) either with HA-Ndfip1 (I) or HA-Ndfip2 (J) (in red) results in redistribution of Robo1 into endosomes and reduced plasma membrane staining.

(K) Cell lysates from COS-7 cells expressing Myc-hRobo1 and HA-tagged Ndfip proteins immunoprecipitated with anti-Myc antibody and analyzed using western blot. Immunoprecipitates were probed with anti-HA, and the inputs (10% of total cell lysate used in the immunoprecipitation step) were analyzed using the indicated antibodies. Both Ndfip1 and Ndfip2 are detected in Robo1 immunoprecipitates in Cos cell lysates.

Error bars represent SEM. Significance was assessed using Student's t test (*$p < 0.05$ and **$p < 0.01$). Scale bar represents 10 μm.

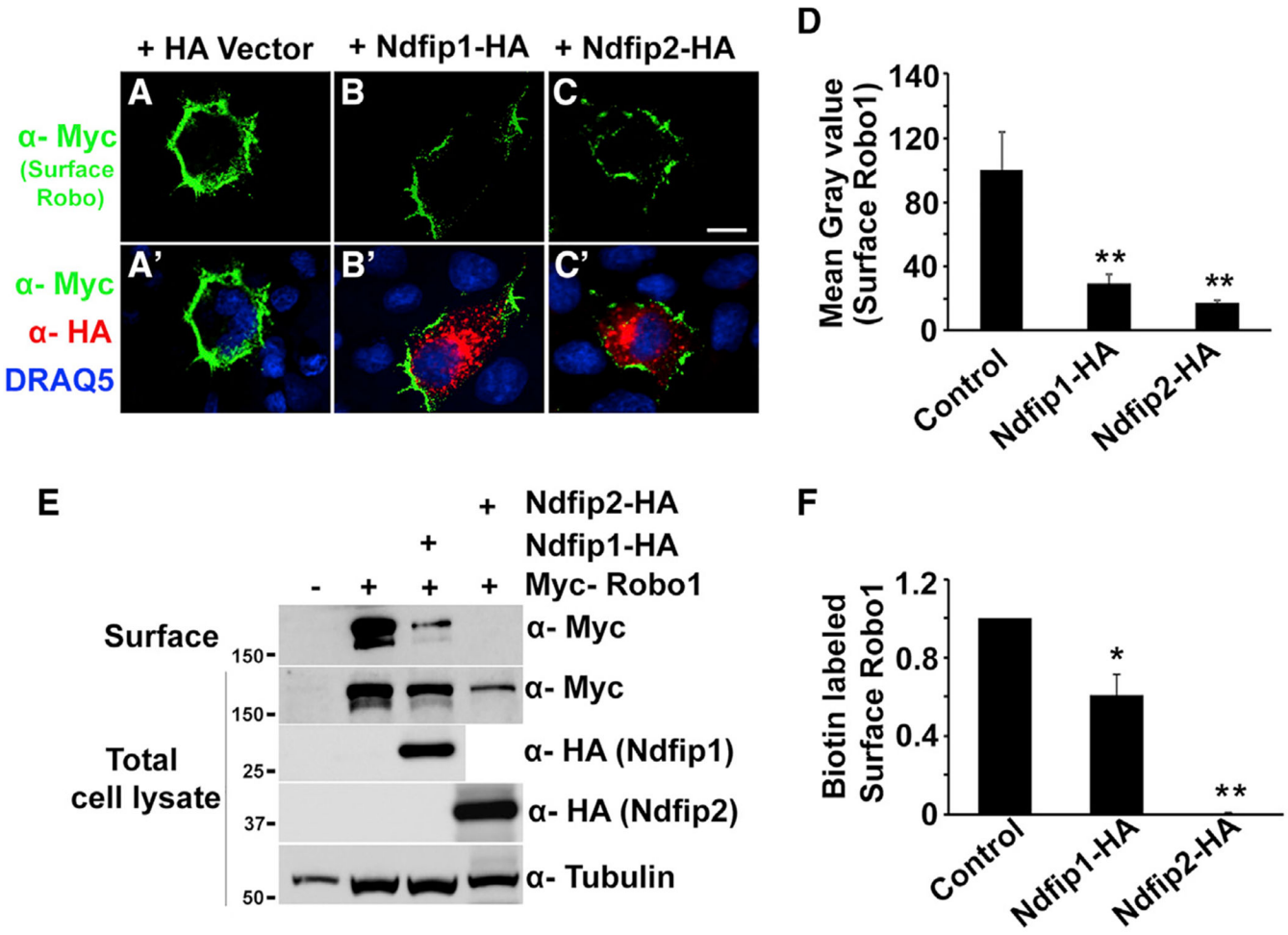

Figure 2. Ectopic Expression of Ndfip1 or Ndfip2 Decreases Robo1 Surface Levels *In Vitro*

(A–C′) Confocal micrographs of COS-7 cells expressing N-Myc-Robo1 with empty HA-vector (A and A′) or with Ndfip1-HA (B and B′) or with Ndfip2-HA (C and C′). Surface expression of Robo1 was visualized by staining the N-terminal Myc tag before fixation and permeabilization (A–C, green). The HA staining reveals the expression of Ndfip1 (B′, red) and Ndfip2 (C′, red). DRAQ-5 is a nuclear marker. Co-expression of Ndfip1 or Ndfip2 with Robo1 leads to a significant decrease in Robo1 at the cell surface.

(D) The fluorescent intensity of surface Robo1 is measured as a mean gray value. Error bars represent SEM. Control, n = 8; Ndfip1-HA, n = 10; Ndfip2-HA, n = 12 (n, number of cells scored for each transfection) (Ndfip1, 29.8 ± 5.74; Ndfip2, 17.6 ± 1.33; $p < 0.001$). Significance was assessed using Student's t test (**$p < 0.001$).

(E) HeLa cells transiently transfected with Myc-Robo1 and Ndfip1-HA or Ndfip2-HA plasmids. 48 h after transfection, cell surface proteins isolated using biotinylation were analyzed using western blot using anti-Myc antibody (top panel). Levels of total Robo1 and the expression of Ndfip proteins were analyzed using western blot using anti-Myc and anti-HA antibodies, respectively. An anti-Tubulin antibody was used to control for equal protein loading. Biotinylated surface Robo1 levels are strongly reduced in Ndfip1 and Ndfip2 transfected cells (Ndfip1: 0.60 ± 0.103, $p = 0.022$; Ndfip2: 0.006 ± 0.004; $p = 0.0014$).

(F) Quantitative representations for biotinylated surface Robo1 band intensities in control vector and Ndfip1-HA- and Ndfip2-HA-transfected cells. Data were normalized to control. Error bars represent SEM. Significance was assessed using Student's t test (*$p < 0.05$ and **$p = 0.001$). Scale bar represents 10 μm.

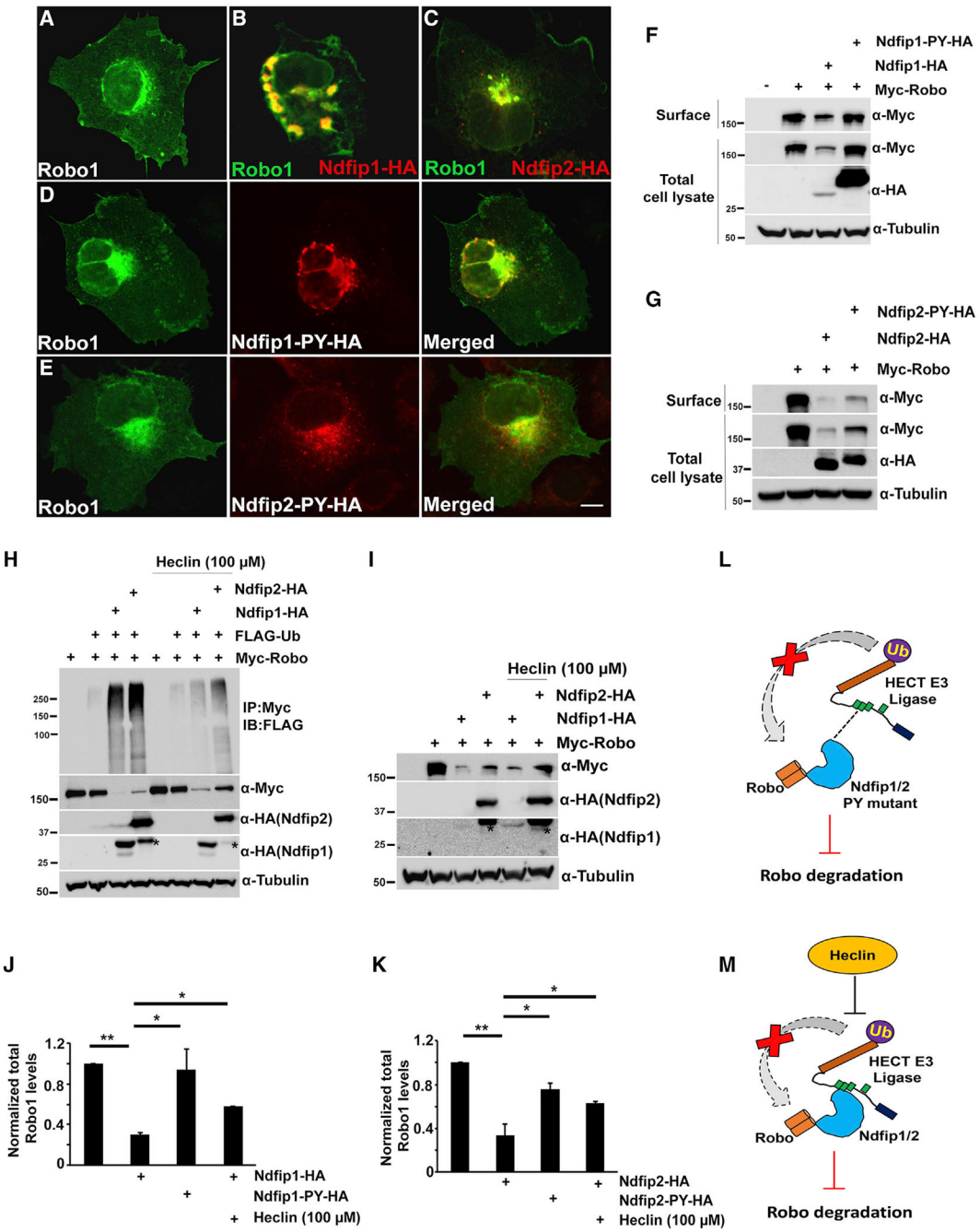

Figure 3. Ndfip PY Motifs and E3 Ligase Activity Are Required for Robo1 Degradation

(A–C) Confocal micrographs of COS-7 cells expressing Myc-tagged Robo1 and HA-tagged Ndfip1 or Ndfip2 with mutations in the PY motifs.

(A) Robo1 (in green) is localized mainly at the plasma membrane and Golgi apparatus in cells that co-expressed a vector control.

(B and C) Co-transfection of Robo1 with either Ndfip1 (B) or Ndfip2 (C) (red) re-localizes Robo1 into endosomes.

(D and E) Co-transfection of Robo1 with either Ndfip1^{PY} (D) or Ndfip2^{PY} (E) does not alter Robo1 localization.

(F and G) COS-7 cells were transfected with plasmids expressing Myc-tagged Robo1 and either HA-tagged Ndfip1 or Ndfip1^{PY} (F), or HA-tagged Ndfip2 or Ndfip2^{PY} (G) as indicated. PY mutant indicates Ndfip versions in which each PY motif was mutated from PxY to PAG. 48 h after transfection, cell surface proteins isolated using biotinylation were analyzed using western blot using anti-Myc antibody. Co-expression of Ndfip1 or Ndfip2 strongly reduces both surface and total Robo1 protein levels, but co-expression of either Ndfip1 ^{PY} or Ndfip2^{PY} does not (Ndfip1: 0.3 ± 0.01, $p < 0.001$; and Ndfip1-PY: 0.94 ± 0.19, $p < 0.05$; Ndfip2: 0.33 ± 0.10, $p = 0.012$; Ndfip2-PY: 0.75 ± 0.05, $p < 0.05$).

(H and I) COS-7 cells were transiently co-transfected with Myc-Robo1, FLAG-Ub, HA-Ndfip1, and HA-Ndfip2 expression constructs as indicated. After 48 h of transfection, cells were treated with 100 μM Heclin for 2 h.

(H) Cell lysates were immunoprecipitated with anti-Myc antibody, and immunoprecipitates were western-blotted with anti-FLAG antibody. Ubiquitylated Robo1 is strongly reduced upon Heclin treatment. Ubiquitylated forms appear as smears.

(I) Robo1 protein is stabilized in Ndfip1 and Ndfip2 transfected cells that were treated with Heclin (Ndfip1 with Heclin: 0.57 ± 0.004 versus Ndfip1: 0.3 ± 0.01, $p < 0.05$; Ndfip2 with Heclin: 0.63 ± 0.01 versus Ndfip2: 0.33 ± 0.10, $p < 0.05$). The expression levels of both Ndfip proteins and Robo1 were analyzed using western blot using anti-HA and anti-Myc antibodies. An anti-Tubulin antibody was used to control for equal protein loading.

(J and K) Quantification of total Robo protein levels in cells expressing Ndfip1 (J) or Ndfip2 (K) proteins with mutations in the PY motifs or in cells treated with Heclin. Data were normalized to tubulin levels. Error bars represent SEM. Significance was assessed using Student's t test (*$p < 0.05$ and **$p < 0.001$).

(L and M) Schematic illustrations demonstrating the mechanism and the effect of PY mutations in Ndfip proteins (L) or Heclin treatment (M) on Robo protein levels.

Scale bars in (A)–(E) represent 10 μm.

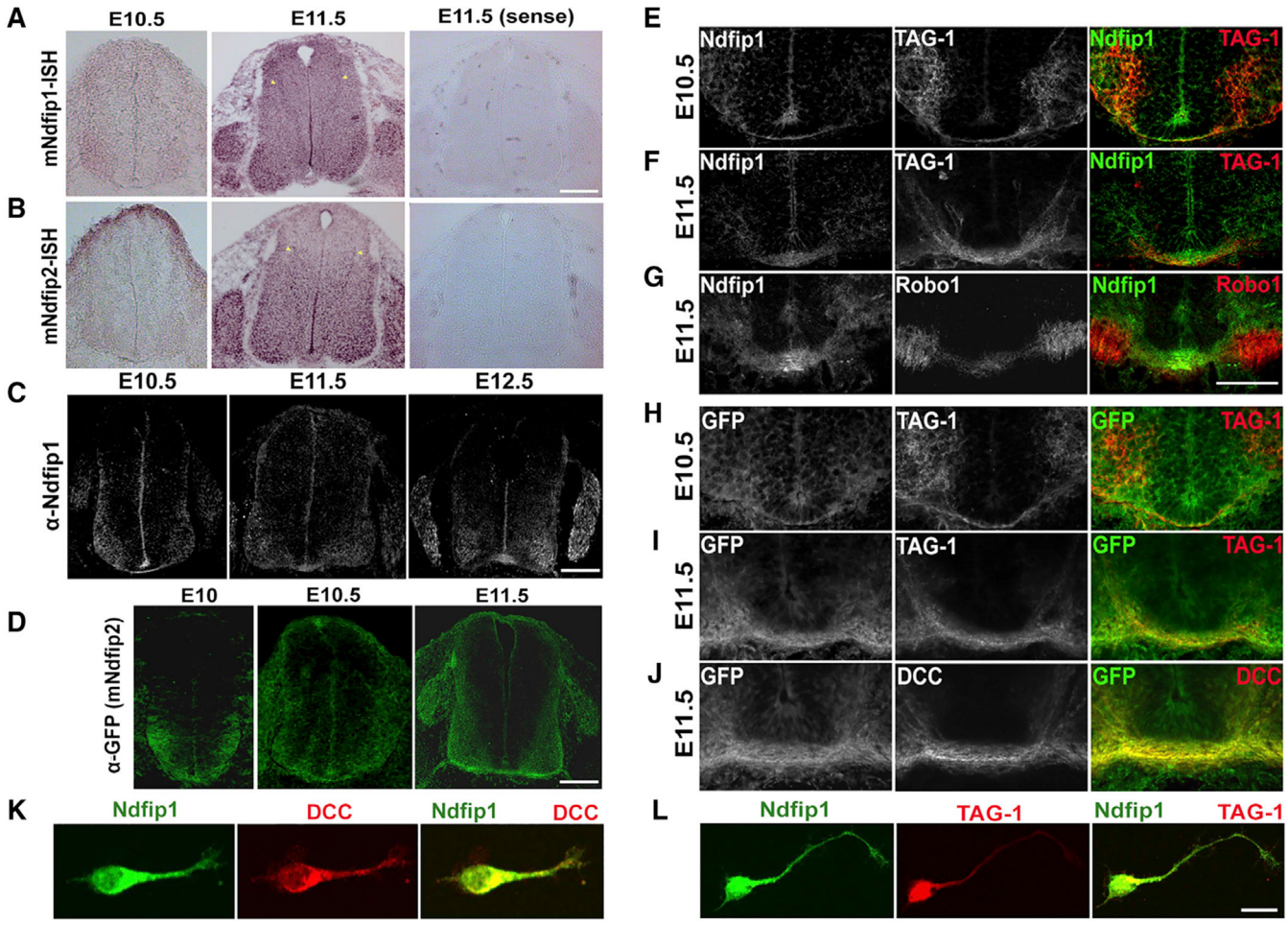

Figure 4. Ndfip1 and Ndfip2 Expression in the Developing Spinal Cord

(A and B) mRNA *in situ* hybridization reveals clear expression of Ndfip1(A) and Ndfip2 (B) in E10.5 and E11.5 mouse spinal cord. mRNA probes to the sense strand serve as controls for the specificity of Ndfip1 (A) and Ndfip2 (B) expression. Yellow arrows in the E11.5 images show expression in regions of dorsal commissural axon cell bodies.

(C) Representative confocal images of transverse sections of wild-type mouse spinal cord from E10.5 to E12.5 labeled with anti-Ndfip1 antibody. Ndfip1 is expressed at the floor plate, in the motor column, and in DRGs.

(D) Anti-GFP immunostaining of E10, E10.5, and E11.5 of embryos reveals the pattern of Ndfip2 expression. Embryos are heterozygous for an allele of Ndfip2 where the coding sequence has been replaced by a GFP reporter. Commissural axons are clearly labeled by E11.5.

(E–G) Higher magnification images of E10.5 and E11.5 spinal cord sections illustrate co-labeling of Ndfip1 and TAG1 (E and F) or Robo1 (G) in the ventral commissure. Co-localization of Ndfip1 with TAG1-positive commissural axons demonstrates the commissural axonal expression of Ndfip1.

(H–J) Higher magnification of anti-GFP immunostaining of E10.5 and E11.5 of Ndfip2-GFP heterozygous embryos reveals co-labeling of Ndfip2 and TAG1 (H and I) or DCC (J) in the ventral commissure.

(K and L) Double immunostaining of Ndfip1 (K and L, green) and DCC (K, red) or TAG1 (L, red) in dissociated commissural neurons showing the expression of Ndfip1 in the cell body, axon and growth cone of commissural neurons.

Scale bars represent 50 μm in (A)–(D), 20 μm in (E)–(J), and 10 μm in (K) and (L).

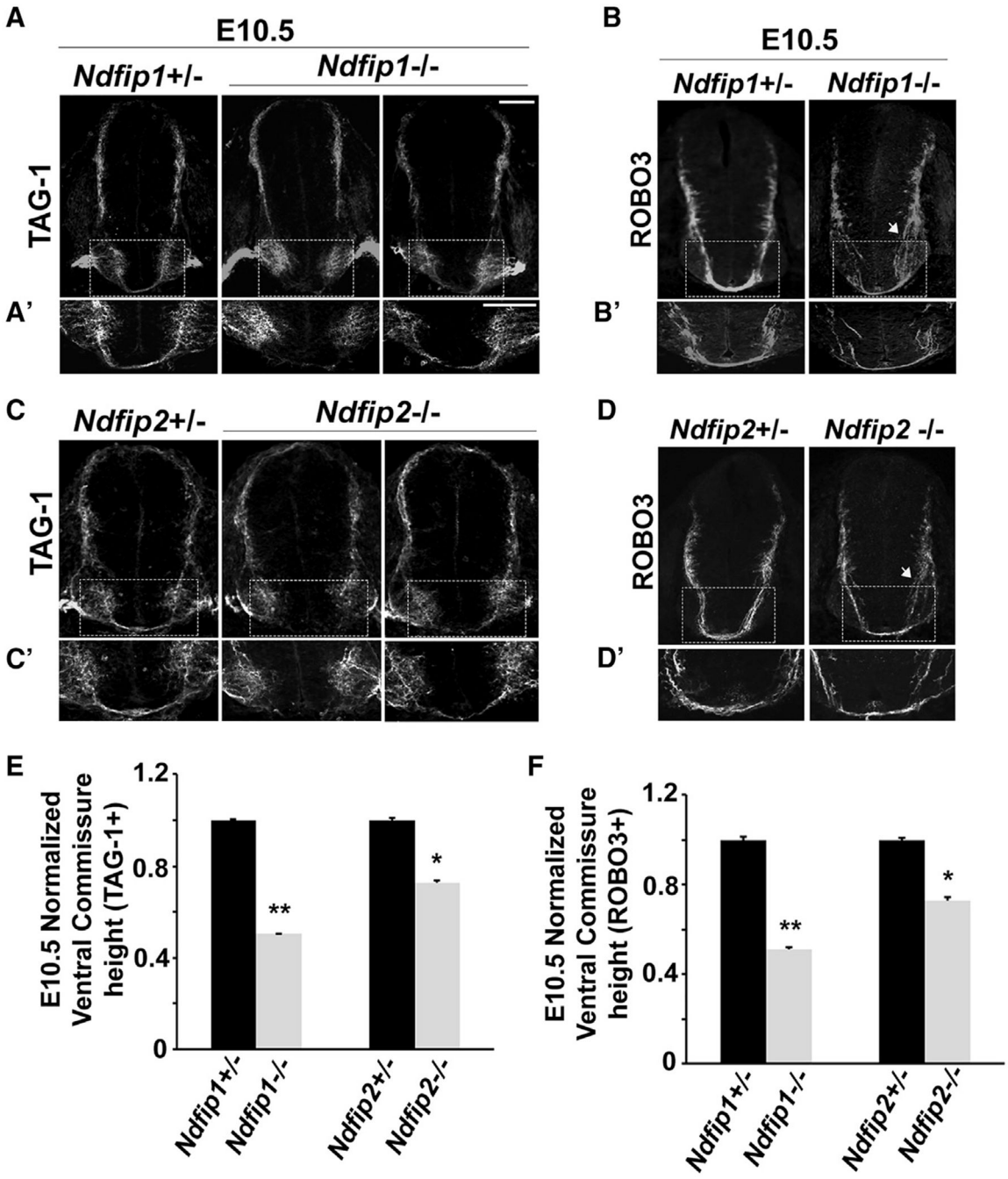

Figure 5. *Ndfip1* and *Ndfip2* Mutant Embryos Have Defects in Midline Crossing

(A–D) Representative confocal images of E10.5 transverse spinal cord sections that were taken from *Ndfip1* or *Ndfip2* heterozygous or mutant littermate mouse embryos. All sections were processed for immunohistochemistry for TAG1 and Robo3.

(A′–D′) Bottom rows show the ventral commissure bundle at higher magnification.

(A and C) *Ndfip1* (A) and *Ndfip2* (C) mutant embryos have a much reduced or no TAG1-positive ventral commissure at E10.5.

(B and D) Cross sections of E10.5 heterozygous or mutant *Ndfip1* (B) and *Ndfip2* (D) embryos stained with Robo3. *Ndfip1* and *Ndfip2* mutant embryos have a reduced Robo3-positive ventral commissure at E10.5. Robo3-positive axons are defasciculated at E10.5 (arrows) with a few axons observed in the motor column in E10.5 *Ndfip1* mutant embryos. (E and F) Quantification of TAG1-positive (E) and Robo3-positive (F) commissure thickness at E10.5. The thickness of the axon bundle at the ventral midline is represented as commissure size in wild-type and *Ndfip1* or *Ndfip2* mutant embryos. In order to control for any variation in size of the embryos, the values of commissure thickness were normalized with the length of the spinal cord (distance between the floor plate and roof plate using ImageJ). Data were normalized to sibling controls. There was a significant reduction in either TAG1- or Robo3-positive commissural axon bundle thickness at the ventral midline at E10.5. The quantifications show the mean and SEM of five to eight sections per embryo, with n = 3 embryos for *Ndfip1* heterozygotes and mutants, n = 3 embryos for *Ndfip2* heterozygotes, and n = 4 for *Ndfip2* mutants.
(A) *Ndfip1* mutant, TAG1+ (0.5 ± 0.003, $p = 0.0024$); (B) *Ndfip1* mutant Robo3+ (0.50 ± 0.006 $p = 0.0058$); (C) *Ndfip2* mutant, TAG1+ (0.72 ± 0.008, $p = 0.032$); and (D) *Ndfip2* mutant, Robo3+ (0.72 ± 0.012, $p = 0.015$). Significance was assessed using Student's t test (**$p < 0.01$ and *$p < 0.05$). Scale bars represent 50 μm in (A)–(D) and 20 μm in (A′)–(D′).

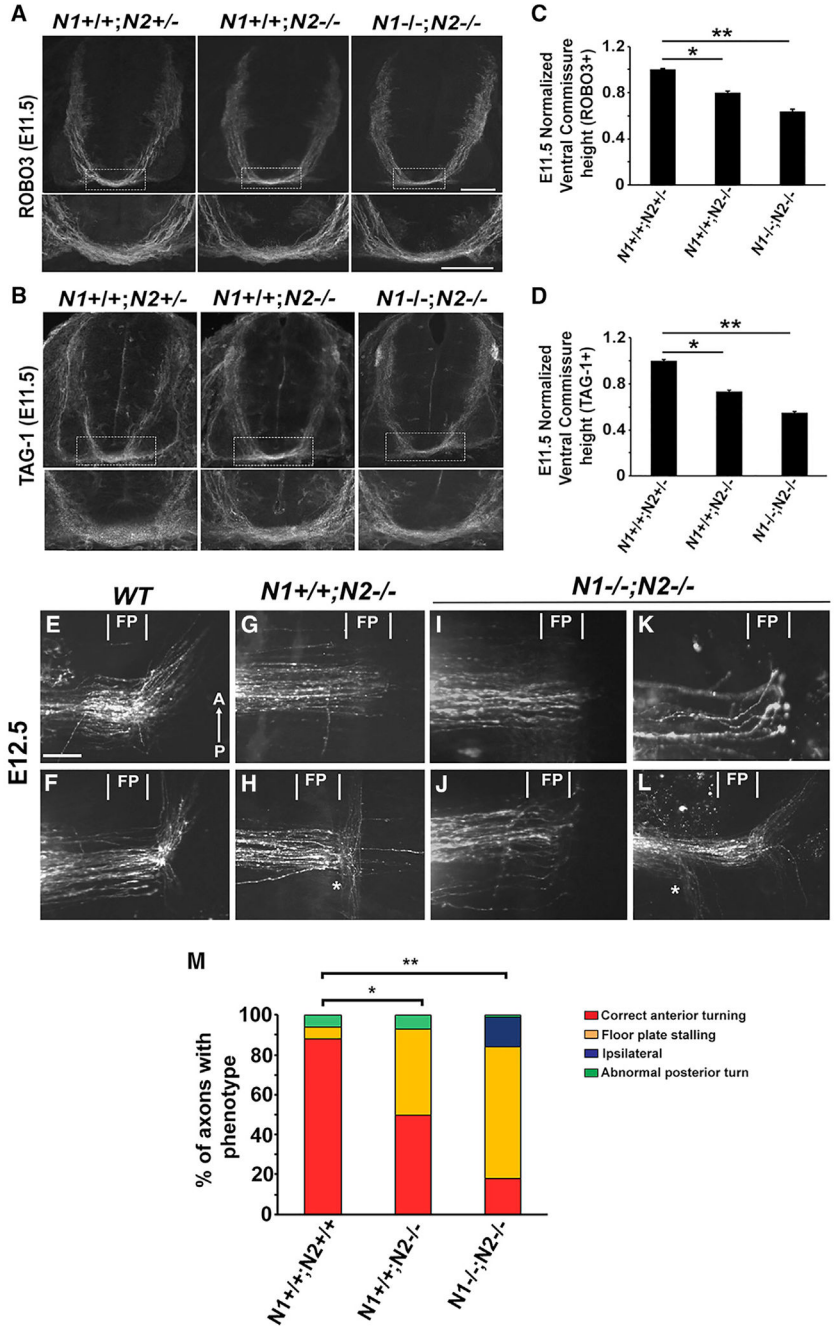

Figure 6. Commissural Axon Guidance Defects in *Ndfip* Double Mutants

(A and B) Representative confocal images of E11.5 transverse spinal cord sections that were taken from *Ndfip2*$^{+/-}$ or *Ndfip2*$^{-/-}$ or *Ndfip1*$^{-/-}$; *Ndfip2*$^{-/-}$ mouse embryos. All sections were processed for immunohistochemistry for Robo3 (A) and TAG1 (B). Bottom rows show the ventral commissure bundle at higher magnification. *Ndfip1*$^{-/-}$; *Ndfip2*$^{-/-}$ mutant embryos exhibit significant reduction in ventral commissure thickness compared with *Ndfip2*$^{-/-}$ and *Ndfip2*$^{+/-}$ embryos.

(C and D) Quantification of Robo3-positive (C) and TAG1-positive (D) commissure thickness normalized with the length of the spinal cord at E11.5 in *Ndfip2*$^{+/-}$ or *Ndfip2*$^{-/-}$ or *Ndfip1*$^{-/-}$; *Ndfip2*$^{-/-}$ mouse embryos. Robo3+ commissure thickness in *Ndfip2*$^{-/-}$ (0.8 ± 0.013, p = 0.0015) and *Ndfip1*$^{-/-}$; *Ndfip2*$^{-/-}$ (0.6 ± 0.014, p < 0.0001) and TAG1 + commissure thickness in *Ndfip2*$^{-/-}$ (0.73 ± 0.012, p = 0.0004) and *Ndfip1*$^{-/-}$; *Ndfip2*$^{-/-}$ (0.55 ± 0.008, p < 0.0001). The quantifications show the mean and SEM of five to eight sections per embryo, with n = 3 embryos were analyzed for each indicated genotype.
(E–L) Confocal images of Dil injections in E12.5 spinal cord open-book preparations labeling commissural axons. The majority of axons in open-book preparations of wild-type embryos cross the floor plate and turn anteriorly on the contralateral side (E and F). In contrast, labeled axons in *Ndfip2*$^{-/-}$ spinal cords frequently stop short and fail to make the correct anterior turn (G). In a few embryos, we also observed that some axons take an abnormal posterior turn in *Ndfip2* mutant spinal cords (denoted with asterisk in H).
(I–L) In *Ndfip1*$^{-/-}$; *Ndfip2*$^{-/-}$, these phenotypes are significantly stronger than those observed in the Ndfip2 single-mutant cords (G and H). In addition to stalling phenotypes, we sometimes observe ipsilateral mis projections in *Ndfip1*$^{-/-}$; *Ndfip2*$^{-/-}$ spinal cords (denoted with asterisk in L).
(M) The graph represents the percentage of the axons with the indicated phenotype. The percentage of axons that turned anteriorly is significantly decreased in *Ndfip2*$^{-/-}$ and *Ndfip1*$^{-/-}$; *Ndfip2*$^{-/-}$ mouse embryos compared with wild-type control. Percentage of axons that turned anteriorly in *Ndfip2*$^{-/-}$ (50% ± 0.40, p = 0.0016) and in *Ndfip1*$^{-/-}$; *Ndfip2*$^{-/-}$ (18% ± 0.34, p < 0.0001). Wild-type; n = 4 with number of injection sites 17, *Ndfip2*$^{-/-}$; n = 5 with number of injection sites 22, *Ndfip1*$^{-/-}$; *Ndfip2*$^{-/-}$; n = 3 with number of injection sites 11 (n, number of embryos analyzed for each genotype). Significance was assessed using Student's t test (**p < 0.0001 and *p < 0.01). FP, floor plate. Scale bars represent 50 μm in (A) and (B); higher magnification images in (A) and (B) are 20 μm and 20 μm in (E)–(L).

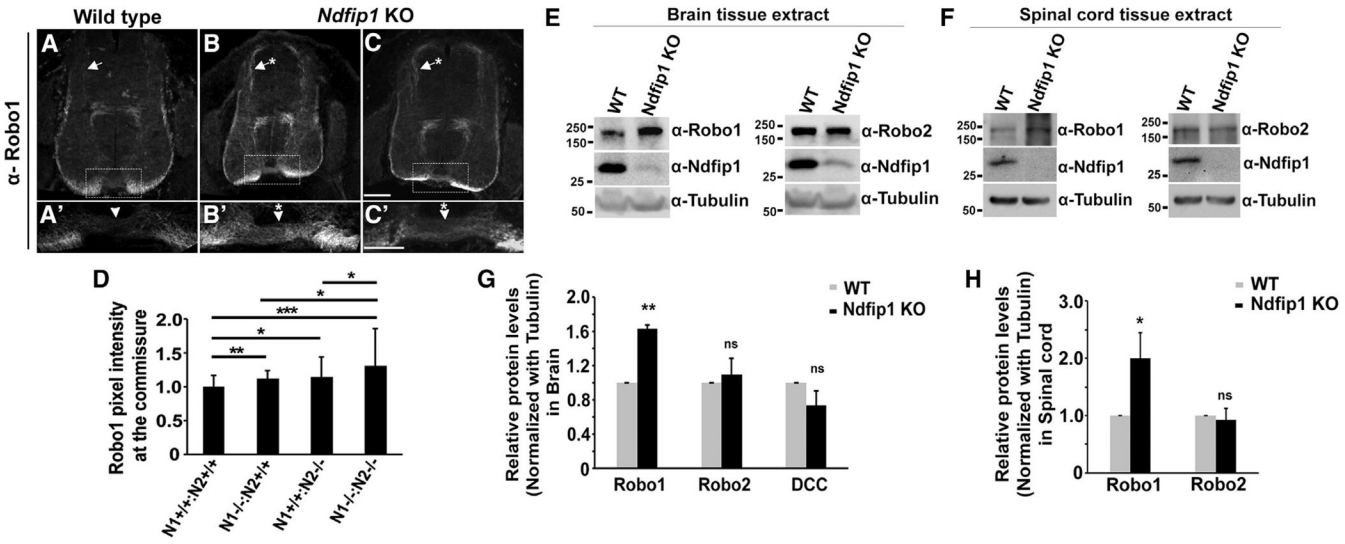

Figure 7. Robo1 Expression Is Increased in *Ndfip* Mutants

(A–C′) Immunohistochemistry against Robo1 protein labels post-crossing axons and pre-crossing (arrow mark) and crossing commissural axons (arrowhead). At E11.5, in *Ndfip1* mutant spinal cord, Robo1 levels are increased in pre-crossing commissural axons (B and C, arrow with asterisk) compared with wild-type (A, arrow). Robo1-positive axons are observed crossing the midline in *Ndfip1* mutant embryos (B′ and C′, arrowhead with asterisk) (n = 4; n, number of embryos). The variability of Robo1 expression in *Ndfip1* mutant embryos is represented in (B) and (C).

(B′ and C′) Higher magnification images at the floor plate region.

(D) Quantitative representation of Robo1 pixel intensity at the commissure in control, $Ndfip1^{-/-}$, $Ndfip2^{-/-}$, and $Ndfip1^{-/-}$; $Ndfip2^{-/-}$ spinal cord sections.

(E and F) Brain extracts (E) and spinal cord extracts (F) from wild-type and *Ndfip1* mutant adult mice were immunoblotted with anti-Robo1 and anti-Robo2 antibodies. Anti-Tubulin antibody was used as a loading control. Robo1 levels are increased in both *Ndfip1* mutant brain or spinal cord lysates compared with wild-type, whereas Robo2 levels are unaltered.

(G and H) Quantitative representation of band intensities of Robo1, Robo2, and DCC in brain lysates (G) or Robo1 and Robo2 in spinal cord lysates (H) that were normalized with tubulin levels.

Error bars represent SEM. Significance was assessed using Student's t test (*$p < 0.05$ and **$p < 0.01$); ns, non-significant. Scale bars represent 50 μm in (A)–(C) and 20 μm in (A′)–(C′).

KEY RESOURCES TABLE

REAGENT or RESOURCE	SOURCE	IDENTIFIER
Antibodies		
Mouse anti-Myc, 1:1000, WB	DSHB	Cat#9E10-C
Mouse anti-HA, 1:1000, IF & WB	BioLegend	Cat#901502
Mouse anti-beta tubulin, 1:1000, WB	DSHB	Cat#E7-S
Rabbit anti-Integrinβ1,1:1000,WB	Cell Signaling Technology	Cat#4706S
Mouse anti-FLAG, 1:1000,WB	Sigma Aldrich	Cat#F1804-50UG
Rabbit anti-Myc, 1:200, IP	Millipore	Cat#06-549
Mouse anti-NDFIP1 (D-4), I:50 (IP) & 1: 300 (WB)	Santa Cruz Biotechnology	Cat#sc-398469
Mouse anti-NDFIP2 (E-4), I:50 (IP) & 1: 300 (WB)	Santa Cruz Biotechnology	Cat#sc-376259
Rabbit anti-Myc, 1:500, IF	Sigma Aldrich	Cat#C3956-2MG
DRAQ5	Cell Signaling Technology	Cat#4084S
Rabbit anti-NDFIP1,1:100 (IHC) & 1:300 (WB)	Sigma Aldrich	Cat#HPA009682
Mouse anti-TAG1, 1:100 (IHC&IF)	DSHB	Cat#4D7/TAG1-C
Goat anti-Robo3, 1:200 (IHC)& 1:1000 (WB)	R & D systems	Cat#AF3076
Goat anti-Robo2, 1:500,WB	R & D systems	Cat#AF3147
Goat anti-Robo1, 1:200 (IHC) & 1:500 (WB)	R & D systems	Cat#AF1749
Goat anti-DCC, 1:400 (IHC)& 1:500 (WB)	R & D systems	Cat#AF844
Rat anti-L1CAM, 1:300 (IHC)	Millipore	Cat#MAB5272
Rabbit anti-GFP, 1:1000, IHC	Invitrogen	Cat#A11122
Goat anti-Mouse HRP, 1:10,000, WB	Jackson Immnuoresearch	Cat#115-035-146
Goat anti-Rabbit HRP, 1:10,000, WB	Jackson Immnuoresearch	Cat#111-035-003
Donkey anti-Goat HRP, 1:10,000, WB	Jackson Immnuoresearch	Cat#705-035-003
Alexa488 Goat anti-Rabbit, 1:500, IHC & IF	Invitrogen	Cat#A11034
Alexa488 Goat anti-Mouse, 1:500, IHC & IF	Invitrogen	Cat#A11029
Alexa633 Goat anti-Rat, 1:500, IHC	Invitrogen	Cat#A-21094
Cy3 Goat anti-Mouse, 1:1000 (IF) & 1:500 (IHC)	Jackson Immnuoresearch	Cat#115-165-003
Cy3 Donkey anti-Goat, 1:500 (IF) & 1:400 (IHC)	Jackson Immnuoresearch	Cat#705-165-003
Chemicals, Peptides, and Recombinant Proteins		
EZ-Link Sulfo-NHS-LC-LC-Biotin	Thermo Scientific	Cat#21338
Neutravidin UltraLink Resin	Thermo Scientific	Cat#53150
MG132	Sigma Aldrich	Cat#M7449-200ul
CQ	Sigma Aldrich	Cat#C-6628
Heclin	Sigma Aldrich	Cat#SML1396
DMSO	Amresco	Cat#WN182-10ML
Dil	Sigma Aldrich	Cat#468495-100MG
DIG RNA labeling mix	Roche Diagnostics	Cat#11277073910
T7 RNA polymerase	Promega	Cat#P207B

REAGENT or RESOURCE	SOURCE	IDENTIFIER
Antibodies		
SP6 RNA polymerase	Promega	Cat#P108B
NBT/BCIP stock solution	Roche Diagnostics	Cat#11383221001
Proteinase K	Roche Diagnostics	Cat#03115828001
Protein A Agarose beads	Invitrogen	Cat#15918-014
rProteinG Agarose beads	Invitrogen	Cat#15920-010
COS-7 cells	ATCC	ATCC CRL-1651
HeLa cells	ATCC	ATCC CCL-2
Experimental Models: Organisms/Strains		
Mouse: Ndfip1	Oliver et al., 2006	N/A
Mouse: Ndfip2	CE O'Leary et al., 2016	N/A
Mouse: CD-1	Charles River	Stock#022
Mouse: C57BL/B6J	Jackson Laboratory	Stock#664
Recombinant DNA		
Plasmid: pCDNA-Myc-hRobo1-V5	This paper	N/A
Plasmid: pCMV-HA-Ndfip1	This paper	N/A
Plasmid: pCMV-HA-Ndfip2	This paper	N/A
Plasmid: pCMV-HA	Addgene	Cat#631604
Plasmid: pCDNA-Myc-Ndfip1	Dr. Thomas Mund lab	N/A
Plasmid: pCDNA-Myc-Ndfip2	Dr. Thomas Mund lab	N/A
Plasmid: pCDNA-HA-Itch	Dr. Thomas Mund lab	N/A
Plasmid: pCDNA-Myc-Ndfip1PY1,2,3	Dr. Thomas Mund lab	N/A
Plasmid: pCDNA-Myc-Ndfip2PY1,2,3	Dr. Thomas Mund lab	N/A
Plasmid: pCMV-HA-Ndfip1PY1,2,3	This paper	N/A
Plasmid: pCMV-HA-Ndfip2PY1,2,3	This paper	N/A
Plasmid: FLAG-Ub	Dr. Hideaki Fujitha lab	N/A
Plasmid: pSectagB-Myc-His-hRobo2	Dr. Weining Lu lab	N/A
Plasmid: pCAGGS/ES-mRobo3.1A-Myc	Dr. Alain Chédotal lab	N/A
Software and Algorithms		
ImageJ Fiji	Fiji	https://fiji.sc/
Adobe Photoshop	Adobe	CS7
Leica SP5 confocal microscope	Leica Microsystems	N/A